



Impact of regional climate change and future emission scenarios on surface O₃ and PM_{2.5} over India

Matthieu Pommier¹, Hilde Fagerli¹, Michael Gauss¹, David Simpson^{1,2}, Sumit Sharma³, Vinay Sinha⁴, Sachin D. Ghude⁵, Oskar Landgren¹, Agnes Nyiri¹, and Peter Wind¹

¹Norwegian Meteorological Institute, Oslo, Norway

²Dept. Space, Earth & Environment, Chalmers University of Technology, Gothenburg, Sweden

³Earth Sciences and Climate Change Division, The Energy and Resources Institute (TERI), New Delhi, India

⁴Dept. of Natural Resources, TERI University, New Delhi, India

⁵Indian Institute of Tropical Meteorology, Pune, India

Correspondence: Matthieu Pommier (matthieu.pommier@met.no)

Received: 2 June 2017 – Discussion started: 17 July 2017

Revised: 30 October 2017 – Accepted: 21 November 2017 – Published: 4 January 2018

Abstract. Eleven of the world's 20 most polluted cities are located in India and poor air quality is already a major public health issue. However, anthropogenic emissions are predicted to increase substantially in the short-term (2030) and medium-term (2050) futures in India, especially if no further policy efforts are made. In this study, the EMEP/MSC-W chemical transport model has been used to predict changes in surface ozone (O₃) and fine particulate matter (PM_{2.5}) for India in a world of changing emissions and climate. The reference scenario (for present-day) is evaluated against surface-based measurements, mainly at urban stations. The evaluation has also been extended to other data sets which are publicly available on the web but without quality assurance. The evaluation shows high temporal correlation for O₃ ($r = 0.9$) and high spatial correlation for PM_{2.5} ($r = 0.5$ and $r = 0.8$ depending on the data set) between the model results and observations. While the overall bias in PM_{2.5} is small (lower than 6 %), the model overestimates O₃ by 35 %. The underestimation in NO_x titration is probably the main reason for the O₃ overestimation in the model. However, the level of agreement can be considered satisfactory in this case of a regional model being evaluated against mainly urban measurements, and given the inevitable uncertainties in much of the input data.

For the 2050s, the model predicts that climate change will have distinct effects in India in terms of O₃ pollution, with a region in the north characterized by a statistically significant increase by up to 4 % (2 ppb) and one in the south by

a decrease up to –3 % (–1.4 ppb). This variation in O₃ is assumed to be partly related to changes in O₃ deposition velocity caused by changes in soil moisture and, over a few areas, partly also by changes in biogenic non-methane volatile organic compounds.

Our calculations suggest that PM_{2.5} will increase by up to 6.5 % over the Indo-Gangetic Plain by the 2050s. The increase over India is driven by increases in dust, particulate organic matter (OM) and secondary inorganic aerosols (SIAs), which are mainly affected by the change in precipitation, biogenic emissions and wind speed.

The large increase in anthropogenic emissions has a larger impact than climate change, causing O₃ and PM_{2.5} levels to increase by 13 and 67 % on average in the 2050s over the main part of India, respectively. By the 2030s, secondary inorganic aerosol is predicted to become the second largest contributor to PM_{2.5} in India, and the largest in the 2050s, exceeding OM and dust.

1 Introduction

Air pollution is a serious health concern in the world and especially over Asia (Atkinson et al., 2012). It has been identified as the fifth most important cause of mortality in India (WHO, 2014). India is among the countries experiencing an increase in the number of high-pollution events during this last decade. With a population of 1.3 billion inhab-

itants, a density of 420 inhabitants per km² (12 times the population density of the United States) and a gross domestic product (GDP) growth of 7.6 % per year in 2015 (www.worldbank.org), India is one of the fastest growing economies in the world. Thus, India has many different challenges to cope with in order to continue its economic development without a negative environmental impact. Nonetheless, air pollution is progressing up in the list of policy priorities.

Heavy air pollution results from a combination of high emissions of pollutants and unfavourable weather conditions. In order to limit air pollution or to regulate the emissions of pollutants, policy measures are starting to be implemented in India at a national level (e.g. National Environment Policy, 2006: http://iced.cag.gov.in/?page_id=1037) or at city level, as in New Delhi, which restricts cars with odd and even license plate numbers (UNICEF, 2016 and references therein) on alternate days. In order to meet clean-air standards for reducing the public health risk and improving air quality in urban areas, the Union Environmental Ministry of Government of India launched a national Air Quality Index as part of a major initiative in 2015 for air pollution mitigation (Ghude et al., 2016).

Changes in air quality are nevertheless not only driven by regulations. Climate change may also have a non-negligible impact on air quality, by modifying atmospheric circulation (e.g. wind speed, mixing depth and transport directions), precipitation, dry deposition, emissions and the chemical production or loss rates of pollutants (e.g. Jacob and Winner, 2009; Fiore et al., 2015). The impact of climate change on air quality has been extensively studied in recent years with regional models (e.g. Langner et al., 2005, 2012; Hedegaard et al., 2008; Simpson et al., 2014; Trail et al., 2014; Lacresonnière et al., 2016) but to our knowledge, no study has been focused on India. Climate change is however a main worry in India, especially in terms of the occurrence and the intensity of extreme events such as floods and cyclones (e.g. Dash et al., 2007; Ministry of Environment and Forests, 2010).

Two of the main pollutants having an impact on air quality and health effects are ozone (O₃) and particulate matter with an aerodynamic diameter lower than 2.5 µm (PM_{2.5}) (e.g. Fann et al., 2012; Silva et al., 2013; Lelieveld et al., 2013, 2015). Ghude et al. (2016) showed that around 570 000 and 31 000 premature deaths were due to PM_{2.5} and O₃ exposure respectively in 2011 – at an economic cost of USD 640 billion, which is a factor of 10 higher than total expenditure on health by public and private expenditure in India.

O₃ is a highly oxidative pollutant formed from precursors. O₃ pollution mostly occurs in summer, due to warmer weather driving photochemical reactions. O₃ levels depend on the balance between reactive nitrogen oxide (NO_x) and volatile organic compounds (VOCs). In the troposphere, the main sink of O₃ is the reaction with the hydroxyl radical (OH) through HO_x reactions (e.g. Crutzen et al., 1999).

In the atmospheric boundary layer, dry deposition (uptake by vegetation) is usually the dominant sink (e.g. Monks et al., 2015).

O₃ is known to be associated with respiratory morbidity and mortality (e.g. Jerrett et al., 2009; Orru et al., 2013) but has increased strongly in Asia in recent decades with industrialization and urbanization (e.g. Cooper et al., 2014). Long-term exposure to high concentrations of surface O₃ can also damage vegetation with substantial reductions in crop yields and crop quality (e.g. Morgan et al., 2006; Mills et al., 2011; Ainsworth et al., 2012). The extent of crop damage in India has been estimated at 3.5 million tonnes a year (Ghude et al., 2014) – sufficient to feed about 94 million people living below the poverty line in India.

PM_{2.5} consists of both primary and secondary components. Primary PM_{2.5} components include organic matter (OM), elemental carbon (EC), dust, sea salt (SS) and other compounds. Secondary PM_{2.5} comprises compounds formed through atmospheric processing of gas-phase precursors. This includes various compounds such as nitrate (NO₃⁻) from NO_x, ammonium (NH₄⁺) from ammonia (NH₃), sulfate (SO₄²⁻) from sulfur dioxide (SO₂), and a large range of secondary organic aerosol (SOA) compounds from both anthropogenic and biogenic VOCs. Important sources of both primary and secondary PM_{2.5} emissions in India are domestic heating in winter, wood burning (mainly used for cooking), road transport with contributions from both exhaust (mostly diesel) as well as non-exhaust emissions from brake and tyre wear, and industrial combustion. The main sink of PM_{2.5} is wet deposition, associated with rain-out and wash-out by precipitation.

Long-term exposure to elevated PM_{2.5} levels leads to increased risk for a variety of diseases, such as cardiovascular disease and respiratory diseases (Lim et al., 2012). The World Health Organization (WHO) states a guideline value of 10 µg m⁻³ annual mean concentration (25 µg m⁻³ for the daily mean) that should not be exceeded in order to ensure healthy conditions. Moreover, the Global Burden of Disease (GBD) study (Forouzanfar et al., 2015) ranked exposure to PM_{2.5} as the seventh most important risk factor contributing to global mortality, responsible for 2.9 million premature deaths in 2013. At the country level, India presents one of the highest population-weighted mean concentrations in the world for 2013 (Brauer et al., 2016).

This study aims to evaluate the effect of the regional climate change and future emissions change in realistic air pollutant emission scenarios, focusing on surface O₃ and PM_{2.5} concentrations. For this purpose, the EMEP/MSC-W chemical transport model (see Sect. 2) was used, hereafter referred to as the EMEP model. In this study we conducted a 10-year simulation of air quality in India driven by downscaled meteorological fields for three periods: 2006–2015 (labelled as the reference), 2026–2035 and 2045–2055. In this study, the

physical and chemical processes that are responsible for the modelled changes are investigated in detail.

Section 2 describes the model set-up. Section 3 focuses on the evaluation of the reference scenario against surface-based measurements. Section 4 highlights the impact of climate change on the level of surface O₃ and PM_{2.5} and Sect. 5 investigates the joint impact of future emission scenarios. The conclusions are provided in Sect. 6.

2 Model set-up

The EMEP model is a 3-D Eulerian model described in detail in Simpson et al. (2012). But for global-scale modelling, some important updates have been incorporated. Although the model has traditionally been aimed at European simulations, global scale modelling has been possible for many years (Jonson et al., 2010, 2015a; Wild et al., 2012). These updates, resulting in EMEP model version rv4.9 as used here, have been described in Simpson et al. (2016) and references cited therein. The main changes concern a new calculation of aerosol surface area (now based upon the semi-empirical scheme of Gerber, 1985), revised parameterizations of N₂O₅ hydrolysis on aerosols, additional gas–aerosol loss processes for O₃, HNO₃ and HO₂, a new scheme for ship NO_x emissions, and the use of new maps for global leaf area (used to calculate biogenic VOC emissions) – see Simpson et al. (2015) for details. The value of the N₂O₅ uptake coefficient ($\gamma_{N_2O_5}$) is very uncertain, but here we use the “Smix-Ten” scheme described in 2015, which seemed to provide the best predictions of O₃ for global O₃ sites with this model version. In addition, the source function for sea salt production was updated to account for whitecap area fractions, following the work of Callaghan et al. (2008).

The domain of each simulation covers the latitudes 5.6–40.7° N and the longitudes 56.2–101.7° E, and the horizontal resolution of the simulations follows the resolution of the meteorological data described in Sect. 2.1. However, the studied region is more centred over India (see Fig. 4b).

As in the standard EMEP model, the boundary conditions for most PM_{2.5} components are defined as prescribed concentrations (Simpson et al., 2015), and O₃ boundary conditions (lateral and top) are defined by the climatological O₃ data from Logan (1998). For dust, concentrations from a global simulation for 2012 (EMEP Status Report 1/2015) have been used as boundary conditions. The influence of the changes in inflow of O₃ or PM_{2.5} from outside the Asian domain is not taken into account.

PM emissions are split into EC, OM (here assumed inert) and the remainder, for both fine and coarse PM. The OM emissions are further divided into fossil-fuel and wood-burning compounds for each source sector. As in Bergström et al. (2012), the OM / OC ratios of emissions by mass are assumed to be 1.3 for fossil-fuel sources and 1.7 for wood-burning sources. The model also calculates windblown dust emissions from soil erosion, but these emissions are negligi-

ble over our studied domain compared to the dust transported from the boundary conditions.

Secondary PM_{2.5} aerosol consists of inorganic sulfate, nitrate and ammonium, and SOA; the latter is generated from both anthropogenic and biogenic emissions (ASOA, BSOA respectively), using the “VBS” scheme detailed in Bergström et al. (2012) and Simpson et al. (2012).

The main loss process for particles is wet deposition, and the model calculates in-cloud and sub-cloud scavenging of gases and particles as detailed in Simpson et al. (2012). Gas and particle species are also removed from the atmosphere by dry deposition. Calculations of O₃ deposition in the EMEP model are rather detailed compared to most chemical transport models. We make use of the stomatal conductance algorithm (now commonly referred to as DO3 SE) originally presented in Emberson et al., 2000, 2001, which depends on temperature, light, humidity and soil moisture. Calculation of non-stomatal sinks, in conjunction with an ecosystem-specific calculation of vertical O₃ profiles, is an important part of this calculation, as discussed in Tuovinen et al. (2004, 2009) or Simpson et al. (2003). The methodology and robustness of the calculations of O₃ deposition and stomatal conductance have been explored in a number of publications (Tuovinen et al., 2004, 2007, 2009; Emberson et al., 2007; Büker et al., 2012).

An initial spin-up of 1 year (2005) was conducted, followed by ten 1-year simulations from 2006 to 2015. Each simulation was used as spin-up of the following year of simulation. The initial spin-up (2005) was excluded from the analysis. To conduct the evaluation on the impact of future climate, similar runs were done with spin-ups of 1 year (2025 and 2045), followed by ten 1-year simulations from 2026 to 2035 and from 2046 to 2055, respectively. In this way, short-term (up to 2030) and medium-term (up to 2050) future climate changes have been analysed. These short-term and medium-term future climate (FC) scenarios used the same anthropogenic emissions as the reference scenario. In addition to the climate change, the impact of the future emission scenarios was investigated by using anthropogenic emissions for the 2030s and the 2050s. These simulations, referred to as future climate and emissions (FCE) scenarios, were run for the same time periods as the FC scenarios, but used emissions for their respective baseline year (2030 for the 2030s and 2050 for the 2050s). In order to simplify the reading, the four future scenarios are named as FC2030, FC2050, FCE2030 and FCE2050.

2.1 Downscaled meteorological data

In this work, the EMEP model used meteorological data from the Norwegian Earth System Model (NorESM1-M, Bentsen et al., 2013). These data were downscaled using the Weather Research and Forecasting (WRF) model version 3.4 following the RCP8.5 scenario (Riahi et al., 2011) for the years 2006–2060. The RCP8.5 combines assumptions about high

population and relatively slow income growth with modest rates of technological change and energy intensity improvements, leading in the long term to high energy demand and greenhouse gas emissions in the absence of climate change policies (Riahi et al., 2011). The method and the evaluation are further detailed in Jackson et al. (2018).

The domain used follows the CORDEX South Asia domain specifications (http://www.cordex.org/index.php?option=com_content&view=article&id=87&Itemid=614), yielding 193 by 130 grid points after removal of a 10-grid-point buffer zone in each direction, on approximately 50 km horizontal resolution and with 30 vertical levels.

The different options used were Thompson microphysics, CAM radiation scheme, Noah Land-Surface Model, Mellor–Yamada–Janjić TKE scheme and the Kain–Fritsch cumulus scheme. The evaluation against ERA-Interim for the temperature and APHRODITE for the precipitation, indicates that the downscaled run has a cold bias especially over the ocean, but when comparing with seven other simulations from the CORDEX South Asia ensemble (also using the RCP8.5 scenario), it still performs among the best over the Indian sub-continent (Jackson et al., 2018). For precipitation, the monsoon season (July–September) was simulated to be too dry, which may be at least partially caused by the too cold Indian Ocean and thus less evaporation. The Western Ghats region receives particularly little precipitation in all seasons, which can be explained by the relatively coarse resolution leading to too little orographic precipitation.

For the future scenarios, NorESM1-M predicts an increase in temperature close to the mean of the CORDEX South Asia ensemble. For many areas there is no consensus concerning the sign of the precipitation change, except during monsoon and post-monsoon periods (October–November) in the 2050s, for which most of the models, including NorESM1-M, predict an increase in precipitation over the major part of India, in comparison with the 2006–2015 period. During the pre-monsoon period (April–June) in the 2050s, half of the models, including NorESM1-M, show a decrease in precipitation, which is larger over the Indo-Gangetic Plains. NorESM1-M also presents this decrease in the 2030s. In winter (December–March), the western coast is characterized by an increase in precipitation, even if this change is lower in NorESM1-M than in the other models (not shown).

2.2 Emissions

Anthropogenic emissions of SO_x , NO_x , CO, PM and non-methane volatile organic compounds (NMVOCs) over India were taken from Sharma and Kumar (2016). These data have a resolution of 36 km \times 36 km and are available for 2011 (used for the reference, the FC2030 and the FC2050 scenarios) and for 2030 and 2050 (used for the FCE2030 and the FCE2050 scenarios, respectively).

For NH_3 (not available from Sharma and Kumar, 2016), and for all areas outside India, anthropogenic emissions from the ECLIPSEv5a baseline data set (http://www.iiasa.ac.at/web/home/research/researchPrograms/air/Global_emissions.html) were used (2010 for the reference, FC2030 and FC2050 scenarios; 2030 for the FCE2030 scenario; 2050 for the FCE2050 scenario). The ECLIPSEv5a baseline emission data set was created with the GAINS model (Greenhouse gas–Air pollution Interactions and Synergies; <http://www.iiasa.ac.at/web/home/research/researchPrograms/GAINS.en.html>) (Amann et al., 2011), which provides emissions of long-lived greenhouse gases and shorter-lived species in a consistent framework.

The anthropogenic emissions used for India are presented in Fig. 1. These future scenarios are characterized by sharp increases in all emissions, even if the CO and the NH_3 emissions increase somewhat less in relative terms (close to 30 % by 2030 and 60 % by 2050) in comparison to the other components. Indeed, the predicted increases between 2011 and 2050 are very large, amounting to 304 % (SO_x), 287 % (NMVOC), 162 % (NO_x and $\text{PM}_{\text{coarse}}$) and 100 % ($\text{PM}_{2.5}$).

The scenario estimating the emissions used by Sharma and Kumar (2016) only incorporates the policies which were already implemented before 2014/15. Thus future road maps of stringent standards in transport and power sectors have been taken into account, but not in the industrial sector. For example, there are no standards for NO_x and SO_2 for many coal-consuming industries. Similarly, despite reduction in biomass-based combustion, there are limited controls over the fugitive NMVOC emissions – which are expected to grow immensely in future. Consequently, the increase in these gases is larger than pollutants like $\text{PM}_{2.5}$, which shows much lesser increase due to interventions taken/planned by the Government of India. Although current policies have likely led to reductions in emission intensities, this may not be enough for controlling absolute emissions in future. This explains the large increase in emissions in contrast to other scenarios described for example in the recent report from the International Energy Agency (IEA, 2016). Indeed, the IEA (2016) forecasts that existing and planned policies in India will help contain pollutant emissions growth in the New Policies Scenario. Thus SO_2 and NO_x emissions each grow by only 10 % by 2040, and by 7 % for the $\text{PM}_{2.5}$ emissions. In their pessimistic scenario, i.e. in the absence of policy efforts, the IEA estimated that SO_2 and $\text{PM}_{2.5}$ emissions would roughly double by 2040 and NO_x emissions would grow almost 2.5 times.

While the NO_x and $\text{PM}_{2.5}$ emissions used hereafter follow the same trend as in the IEA report, the SO_x emissions are projected to increase more, by around 4 times from 2011 to 2050. It is noteworthy that there are differences in economic growth rates assumed in the IEA report and the assessments used in Sharma and Kumar (2016). Sharma and Kumar (2016) assumed higher growth rates for India than

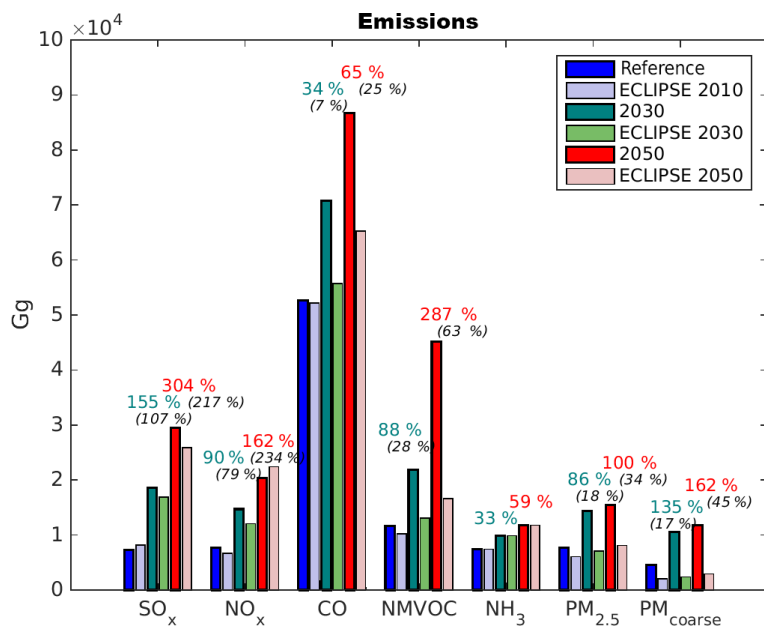


Figure 1. Annual emissions (in Gg yr^{-1}) used for the reference (2010), FC2030 and FC2050 scenarios (dark blue), and for 2030 (dark green) and 2050 (dark red), used for the FCE2030 and the FCE2050 scenarios over India, respectively. The variation of each compound with respect to the reference scenario is also provided by coloured percentage figure. The ECLIPSE emissions are also plotted for comparison and represented by light coloured bars. The variation of each compound with respect to ECLIPSE2010 scenario is also provided by italic black percentage figure given in parentheses.

in the IEA report. This comparison shows that the emissions used in this work reflect a pessimistic scenario. The emissions will continue to grow if no stringent standards are adopted and our FCE scenarios highlight the air quality issue in India without policy effort.

For comparison, the ECLIPSEv5a emissions are also plotted in Fig. 1 since the NH_3 emissions from ECLIPSEv5a were used as complement of the emissions from Sharma and Kumar (2016). The emissions used in this study show larger increase, and the amount of pollutants is also higher for all compounds compared to ECLIPSEv5a, except for NO_x in 2050. It is also interesting to note that the emissions used in the FCE scenarios are higher than the emissions used in the RCP8.5 scenarios for all species over India, except NH_3 (not shown). One of the drawbacks of these RCP8.5 emissions is that only elemental carbon and organic carbon emissions are reported and not $\text{PM}_{2.5}$ and $\text{PM}_{\text{coarse}}$ emissions (e.g. Zhang et al., 2016). Moreover, the RCP scenarios were not developed with a primary focus on air pollution concerns but for greenhouse gases (e.g. Amann et al., 2013).

For the other emissions, biogenic emissions of isoprene and monoterpene are calculated in the model by emission factors as a function of temperature and solar radiation (Simpson et al., 2012). The land-cover data underlying these calculations are from GLC-2000 (<http://forobs.jrc.ec.europa.eu/products/glc2000/glc2000.php>).

The forest fire emissions used correspond to the mean of “Fire INventory from NCAR version 1.5” FINNv1.5 emissions (Wiedinmyer et al., 2014) from 2005 to 2015.

3 Evaluation of the reference simulation with measurements

In this section, we evaluate the levels of the simulated surface O_3 and $\text{PM}_{2.5}$ for the reference scenario to ensure the validity of this scenario. The pollutant concentrations were averaged over their respective decade of simulation. It is important to do this evaluation in order to identify the biases or the errors of the reference runs, and give confidence in the model’s ability to analyse future air quality projections. It should be noted that many factors can affect such evaluations, including accuracy of the emissions, model processes, the quality of the observations, the resolution and the quality of the downscaled meteorological fields, but good agreements found with the reference scenario increase our confidence in predicted concentrations. The details of the statistical numbers are provided in the Appendix.

3.1 O_3

Surendran et al. (2015) presented an evaluation of surface O_3 mixing ratios simulated by the global atmospheric chemistry and transport model MOZART-4 against surface-based measurements. We have used an updated version of this catalogue

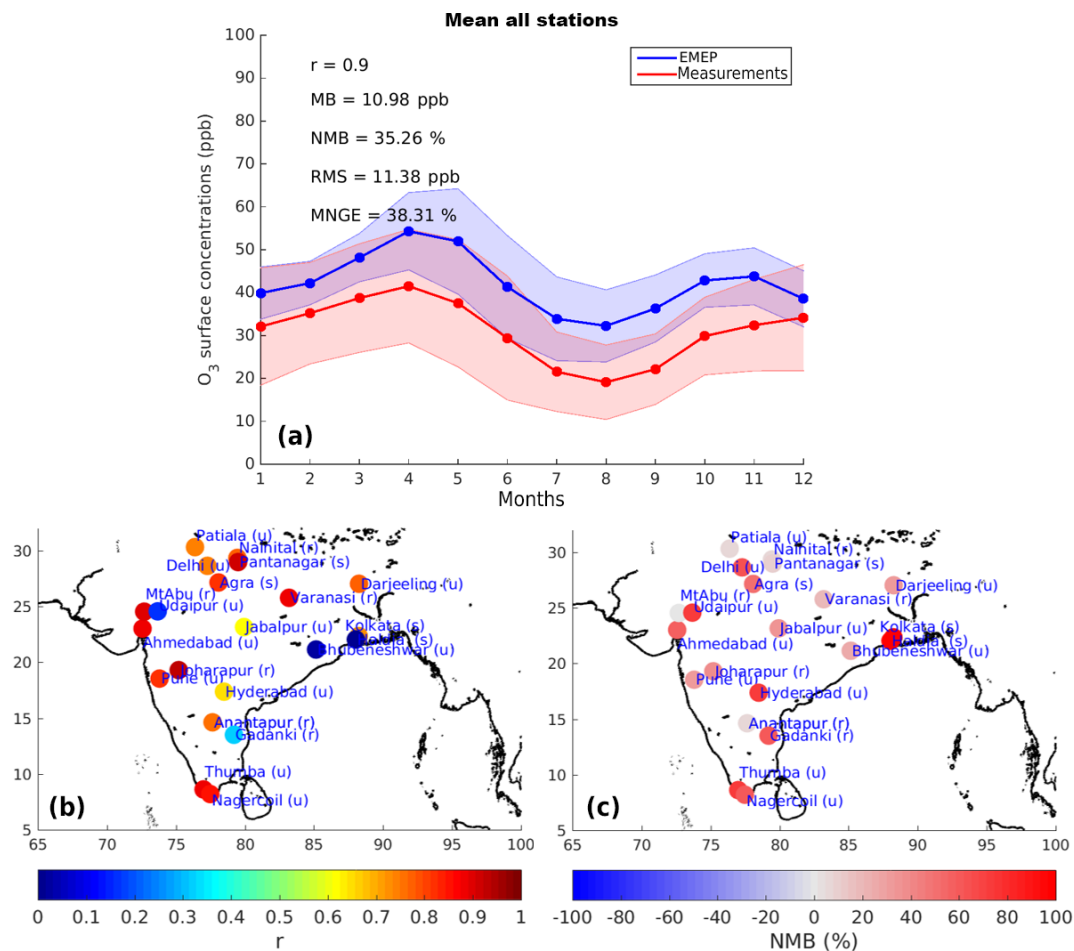


Figure 2. (a) Monthly surface O_3 mean concentrations for the 22 stations (red) and EMEP (averaged over the period of simulation) (blue). EMEP concentrations are collocated to each station. The shade error corresponds to the standard deviation. The correlation coefficient (r), the mean bias (MB), the normalized mean bias (NMB), the root mean square (RMS) error, and the mean normalized gross error (MNGE) are provided. (b) Correlation coefficient for each site. (c) Normalized mean bias for each site. The type of station is given by a letter in parentheses (u , urban; s , suburban; r , rural).

of surface observations. In total, 22 stations were available for this comparison with different periods of measurements as shown in Fig. S1 in the Supplement. This data set corresponds to monthly means over their corresponding period. The discrepancies between the periods of all the stations may have an impact on the evaluation, since the measurements do not necessarily match the emissions year used for the reference scenario. The observations compiled by Surendran et al. (2015) are a mixture of data from the Modelling Air Pollution and Networking (MAPAN) observational network of the Ministry of Earth Sciences (MoES) and from the Indian Institute of Tropical Meteorology (IITM) over urban, suburban and rural sites, with 11, 4 and 7 stations respectively (the individual time-series are shown in Fig. S2).

Averaging the concentrations over all these sites, the simulated O_3 shows a high temporal correlation ($r = 0.9$) with the data set (Fig. 2a). This shows that EMEP captures rather well the seasonal variation of the surface O_3 over the differ-

ent sites but it overestimates the mean value. The mean overestimation is 35 % (11 ppb) but it varies from site to site, between -1.4% and around 130 %. There is no clear geographical pattern to this overestimation or for the temporal correlation (Figs. 2b–c) but the comparison shows the lowest bias for rural sites (15 %) and the highest biases for the urban and suburban sites (Fig. 3), as expected due to the coarse scale of the model and the titration effect discussed below. The overestimation in O_3 found in this work is in agreement with previous studies (e.g. Kumar et al., 2012; Chatani et al., 2014; Sharma et al., 2016), although of course there are many differences in both emissions and models between these studies. It has also been noted that the EMEP model slightly overestimates O_3 , especially with the global version of the model in spring and in winter (e.g. Jonson et al., 2015b). This bias can however be impacted by the parameters used – such as for example the boundary conditions and the emissions. Stadtler et al. (2017), who used PANHAM anthropogenic emissions,

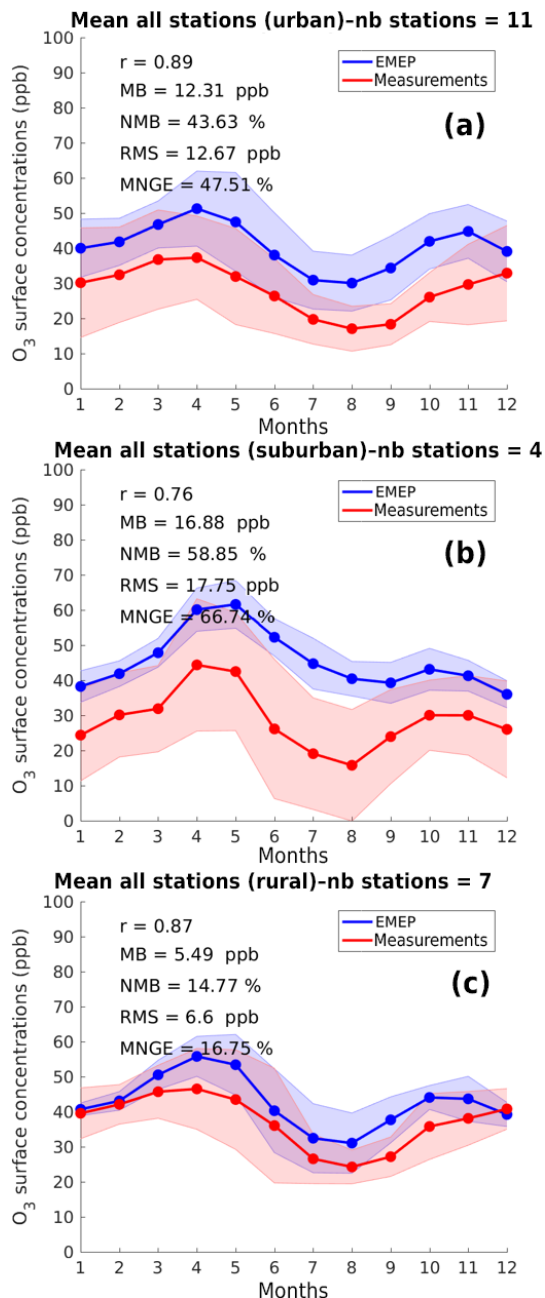


Figure 3. Monthly surface O_3 mean concentrations for the urban (a), suburban (b) and rural (c) stations shown in Fig. 2 (red) and EMEP (averaged over the period of simulation) (blue). EMEP concentrations are collocated to each station. The number of stations is given. The shade error corresponds to the standard deviation. The correlation coefficient (r), the mean bias (MB), the normalized mean bias (NMB), the root mean square (RMS) error, and the mean normalized gross error (MNGE) are provided.

also reported an overestimation in O_3 over different regions such as Asia.

Several hypotheses could explain the overestimation in monthly averaged surface O_3 . These include general uncer-

tainties in anthropogenic and biogenic emissions, an overestimation in the transported O_3 from the boundary conditions (including stratospheric–tropospheric exchange), inadequate accounting for the impacts of the large PM concentrations on gas–aerosol interactions, or systematic biases in the deposition estimates. There is also very likely a misrepresentation of the NO_x – O_3 equilibrium. Under titration conditions (typically when fresh urban NO emissions are reacting with incoming O_3 to create NO_2) an underestimation in NO_2 is associated with an overestimation in O_3 . Sharma et al. (2016) and Chatani et al. (2014) also show overestimation in O_3 by the models mainly due to coarser resolutions which are not able to account for titration chemistry at the local scales. Titration of O_3 with NO can occur over Indian cities (e.g. Sinha et al., 2014; Sharma and Khare, 2017) and is difficult to reproduce in regional models (e.g. Engardt, 2008). There were unfortunately no co-located NO_2 or NO measurements available for this O_3 data set over India. However, a comparison was attempted with NO_2 and O_3 measurements provided by <https://openaq.org> for 2016 over Indian cities and shown in Fig. S3. We only used sites measuring both compounds simultaneously and continuously during all months. Moreover, <https://openaq.org> archives worldwide real-time air quality measurements without validating the data. This highlights the difficulty in evaluating the model results without reliable co-located measurements of trace gases and meteorological parameters. For India, the source of these data is the Central Pollution Control Board of India (CPCB, <http://www.cpcb.gov.in/CAAQM/frmUserAvgReportCriteria.aspx>). As in the comparison with the updated version of O_3 data from Surendran et al. (2015), these observations reflect the O_3 peak around April–May. It also illustrates the underestimation by EMEP in NO_2 surface concentrations and the clear overestimation in O_3 over urban sites. Figure S3 may also suggest that O_x ($NO_2 + O_3$) concentrations are over-predicted. As O_x is conserved under titration reactions, this suggest an overestimate of photochemical activity in the region. Some possible reasons for this might be problems with the anthropogenic and/or biogenic emissions, or over-active chemistry, e.g. over-predictions of photolysis rates for Indian conditions (as EMEP photolysis calculations assume standard atmospheric conditions, and thus do not account for attenuation of radiation due to enhanced aerosols over polluted regions) or problems with heterogeneous reactions. However, it is important to remember that the observations are provided without quality assurance, so data quality may also play a role.

The dilution of the urban emissions into large grid boxes for the urban scale could also partly explain the overestimated O_3 (e.g. Sillman et al., 1990; Pleim and Ching, 1993), especially by considering that downscaled meteorological fields were used at a coarse resolution (50 km) for a comparison at city level. This statement needs however to be tested, because an increased grid resolution does not necessarily lead to a better simulation of O_3 or NO_2 , as explained by Pleim and Ching (1993). Sharma et al. (2017) also con-

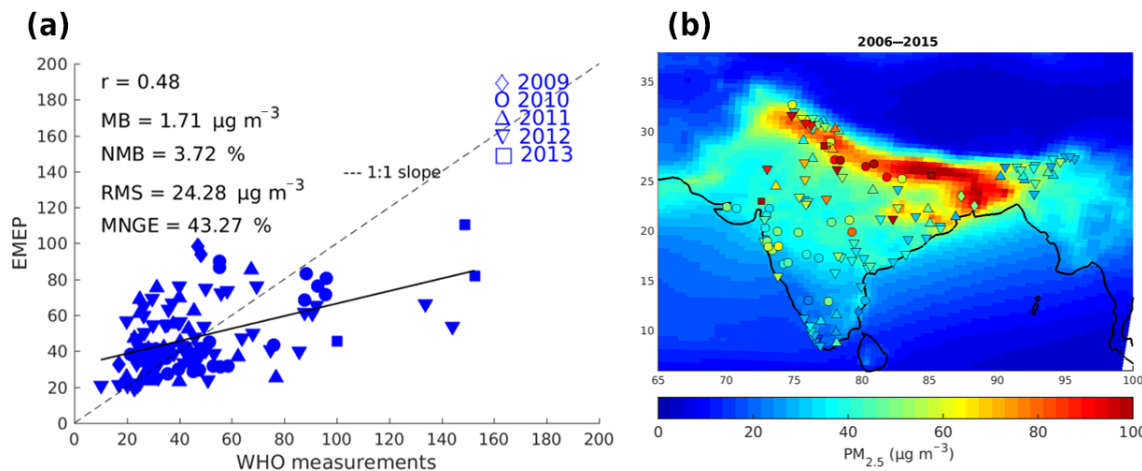


Figure 4. (a) Scatterplot between the surface PM_{2.5} concentrations from EMEP (averaged over the period of simulation) and the concentrations from WHO in $\mu\text{g m}^{-3}$. Data are represented by a different symbol for the corresponding year. The correlation coefficient (r), the mean bias (MB), the normalized mean bias (NMB), the root mean square (RMS) error and the mean normalized gross error (MNGE) are provided. (b) Distribution of the mean surface PM_{2.5} concentrations for the period 2006–2015 (reference scenario). The WHO measurements from 2009 to 2013 are superimposed on the map and represented by coloured symbols following the symbols shown on the scatterplot.

cluded that improving the models' resolutions leads to better performance only to an extent, and may not always show improvement with finer resolutions.

3.2 PM_{2.5}

In contrast to the O₃ evaluation, three different data sets were available for the evaluation of the surface PM_{2.5} concentrations. Two of the data sets correspond to the means over a specific period over Indian cities and are from in situ observations from the CPCB of India. Among these two data sets, one corresponds to the WHO database (http://www.who.int/phe/health_topics/outdoorair/databases/cities/en – database 2015). This is a database containing annual means from 2009 to 2013. The other of these two data sets corresponds to averaged concentrations over the period from 2000 to 2010 published by Dey et al. (2012). The third data set corresponds to hourly measurements at the US embassy and consulates in India available for 2014 (i.e. over New Delhi, Chennai, Kolkata, Mumbai, Hyderabad; available at <https://in.usembassy.gov/embassy-consulates/new-delhi/air-quality-data/>).

As for O₃, this evaluation remains challenging due to the location of each site, i.e. downtown, without information about the representativeness of the measured concentrations for a larger area. Despite the difficulty of comparing urban stations with simulations from a regional model, a fair agreement (spatial correlation of 0.5 and a bias of 4 %) with the data from WHO was found with the simulated surface PM_{2.5} concentrations (Fig. 4a). A better agreement is found for the coastal sites, especially in the south and the east of India (Fig. 4b).

The agreement between the simulated concentrations with observations is largely improved in the comparison with the data provided in Dey et al. (2012) (Fig. 5). The correlation is around 0.8 and the bias is about 6 %. It is worth noting that a few discrepancies are observed between the data sets provided by WHO and by Dey et al. (2012). For example, Dey et al. (2012) presented higher concentrations for the city of Patna than the value published by WHO. It is also probable that a change in the emissions and thus in the observed PM_{2.5} concentrations between the periods of both data sets has an impact on the comparison. Similar patterns are also noted in the measurements. For example, the city of Delhi is characterized by higher observed concentrations in both data sets than the value simulated by the model. The bias from the model can be expected, given its resolution.

Despite the differences in the data sets, comparison with observations shows limited biases from EMEP (even though the mean normalized gross errors are large) and good correlations.

Compared to the five urban sites provided by the US Embassy and consulates, a limited agreement is found (Fig. 6), with an underestimation in PM_{2.5} by EMEP for all sites, especially in winter. This comparison shows however a fair agreement, especially given the large variability in the observations, as over New Delhi on 16 July 2014 with a PM_{2.5} surface concentration ranging from 5 to 955 $\mu\text{g m}^{-3}$. Our reference simulation has also been compared with the data provided by <https://openaq.org> for 2016 (Fig. S4). The observations show a large variability within each month, making the interpretation of this comparison difficult. A chemical speciation in the measurements will be helpful to interpret the biases found over these cities. Indeed, the EMEP model predicts a large contribution from primary particulate matter

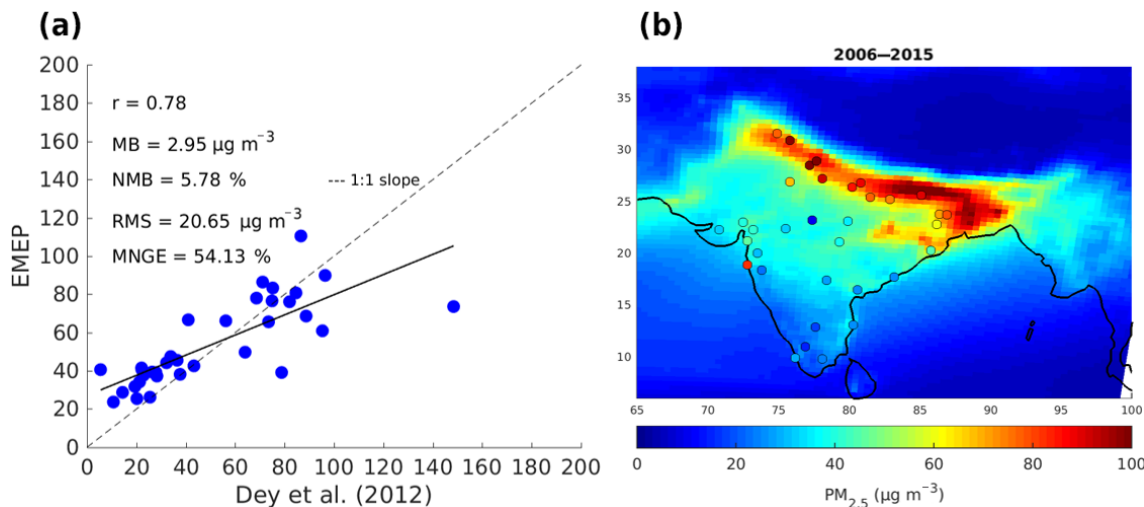


Figure 5. (a) Scatterplot between the surface PM_{2.5} concentrations from EMEP (averaged over the period of simulation) and the concentrations listed in Dey et al. (2012) in $\mu\text{g m}^{-3}$. The correlation coefficient (r), the mean bias (MB), the normalized mean bias (NMB), the root mean square (RMS) error and the mean normalized gross error (MNGE) are provided. (b) Distribution of the mean surface PM_{2.5} concentrations for the period 2006–2015 (reference scenario). The measurements from Dey et al. (2012) are superimposed on the map and represented by coloured dots.

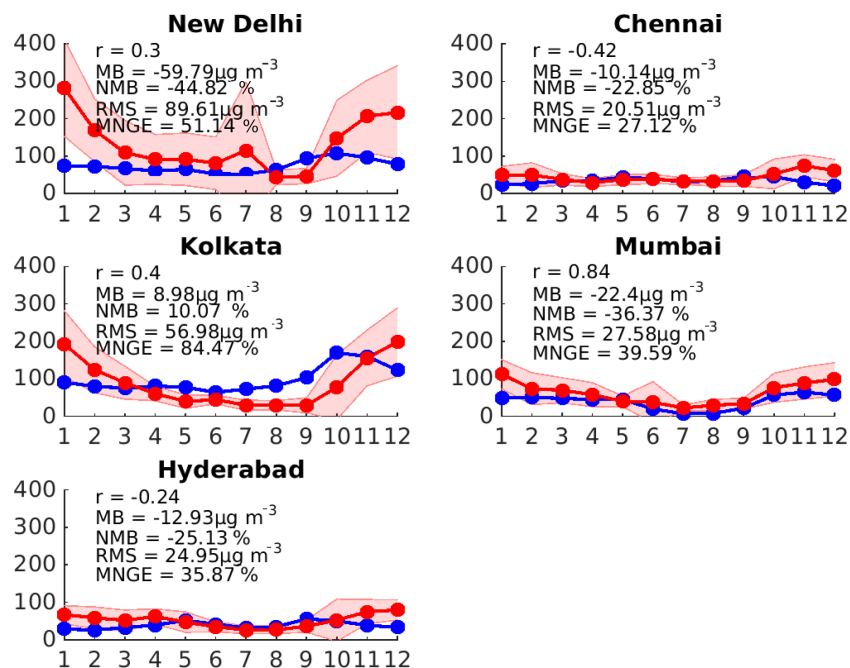


Figure 6. Time series of monthly surface PM_{2.5} mean concentrations in $\mu\text{g m}^{-3}$ for the observations in 2014 (red) and EMEP for the reference scenario (averaged over the period of simulation) (blue) over New Delhi, Chennai, Kolkata, Mumbai and Hyderabad. The red shaded error corresponds to the standard deviation of the measurements. The correlation coefficient (r), the mean bias (MB), the normalized mean bias (NMB), the root mean square (RMS) error, and the mean normalized gross error (MNGE) are provided.

(PPM) to PM_{2.5}, reaching 50 % in December and in January, mainly composed of primary organic matter (not shown), over the sites presented in Figs. 6 and S4. The model also predicts a main natural contribution to PM_{2.5} from May to September over these sites. For example, the site of Hyder-

abad reaches up to 70 % in dust in July. An evaluation of the source attribution of the PM_{2.5} simulated by the EMEP model would be instructive.

Finally, it should be noted that for these simulations, the EMEP model is driven by climate–model meteorology. Such

meteorology is more statistical in nature than the assimilated Numerical Weather Prediction meteorology normally used with the EMEP model, and by its nature (non-assimilated), such climate meteorology cannot reproduce actual meteorology for the periods studied. It is also important to recall that, even with the use of recent inventories, uncertainties in emissions may persist (e.g. Saikawa et al., 2017).

Overall, however, the results suggest that the PM_{2.5} concentrations simulated by the EMEP model with this setup provide a fair representation of the surface concentrations observed at the Indian monitoring sites, even if the model tends to underestimate the highest concentrations and overestimate the lowest ones.

4 Impact of climate

In this section, we analyse the differences between the FC scenarios (at short-term and medium-term, i.e. FC2030 and FC2050) and the reference scenario. All meteorological fields and pollutant concentrations were averaged over their respective decade of simulation. It is important to recall that uncertainties in the representation of meteorological conditions can impact our chemical results even if consistencies in the projections were simulated, especially during the monsoon and pre-monsoon periods, as explained in Sect. 2.1.

4.1 O₃

The reference scenario shows large surface O₃ over Tibet, east India and over the Bay of Bengal along the Indian coast (Fig. 7). The large values seen over Tibet are mainly the result of topographical effects, since O₃ values generally increase with altitude (e.g. Loibl et al., 1994). High O₃ near coastal areas is also expected, since the deposition velocity of O₃ is very low over sea (e.g. Ganzeveld et al., 2009), thus minimizing the near-surface sink which usually affects land areas.

Increased temperatures associated with climate change would be expected to coincide with a rise in surface O₃ due to the correlation between O₃ production and temperature in polluted areas as explained by Jacob and Winner (2009), although such relationships are often weak (Langner et al., 2005, 2012) and less clear in background areas. This correlation is not obvious in our simulated projections, presumably due to the large number of other factors which change, such as humidity levels, mixing heights, other meteorological changes, and biogenic emissions which are affected by climate change. As our model does not include any CO₂ inhibition effect on isoprene emissions (e.g. Guenther et al., 1991; Arneth et al., 2007), or potential changes in vegetation in a different climate, these biogenic emissions are simply a function of temperature and increase in the FC scenarios. The uncertainties associated with these assumptions are however difficult to quantify. For example, Hantson et al. (2017) found global isoprene emissions for the period 2071–2100 to be

544 TgC yr⁻¹ without CO₂ inhibition, but only 377 TgC yr⁻¹ with this effect (i.e. –31 %). For monoterpenes, the equivalent figures were 35.7 and 24.8 TgC yr⁻¹ (also –31 %). Young et al. (2009) estimated even bigger changes for isoprene, from 764 to 346 TgC yr⁻¹, and showed that this uncertainty can indeed have strong effects on surface O₃ levels. The largest changes were found in South America and Africa, though annual changes over India were only around 5–10 %. Although significant, these changes are model estimates only. The experimental data behind the CO₂ inhibition effect are extremely limited, and as noted in Simpson et al. (2014) and references therein, current knowledge is insufficient to make reliable predictions on this issue.

While the regions with a change in O₃ when using the FC2030 scenario are relatively scattered, the use of the FC2050 scenario highlights a clear north–south difference over land (Fig. 7). This is characterized by an increase in surface O₃ concentrations over the northern part of India (by up to 4.4 %, +2 ppb) and a decrease over the southern tip of India reaching –3.4 % (–1.4 ppb) (Fig. 7). The changes are statistically significant at the 95 % level for both FC scenarios showing a robust effect due to the climate change.

The correlation between the temporal change in O₃ (ΔO_3) and ΔT over land is limited in FC2030 and FC2050 scenarios. This shows that for both FC scenarios, even though the change in temperature is statistically significant (not shown), other processes are occurring which impact on the thermal influence on the photochemical production of O₃.

Figure S5 shows the change in one important process, the O₃ deposition velocity, $V_d(O_3)$. The distribution of relative difference in O₃ is linked to the distribution of relative difference in $V_d(O_3)$ for both FC scenarios, especially in the FC2050 scenario. Wu et al. (2012) already identified a slight increase in O₃ deposition in the south of India and over the Western Ghats due to an increase in the leaf area of broadleaf forests but such processes are not included in our model. Instead, the changes in V_d are due to the factors which control stomatal conductance (g_s) in the EMEP model, namely temperature, humidity (vapour pressure deficits), radiation and soil moisture (Emberson et al., 2001; Simpson et al., 2012). In northern European conditions, an increase in temperature will usually result in an increase in g_s , but in India, temperatures are often above the optimum values, and increases in temperatures may decrease g_s . The other factors will also affect the sign of changes in g_s – such as soil moisture, shown in Fig. S6. Figure S6 shows the large impact of changes in soil moisture on the variation in $V_d(O_3)$ for both FC scenarios. The monthly variation in soil moisture matches the variation in $V_d(O_3)$ rather well.

With regard to seasonal changes and focusing on the FC2050 scenario (Fig. 8), where the signatures in the change in O₃ are more significant (similar plots for the FC2030 scenario shown in Fig. S7), the impact of $V_d(O_3)$ is clearly visible. Exceptions are modelled over three regions as annotated in Fig. 8, where they are labelled as (A), (B) and (C) in the

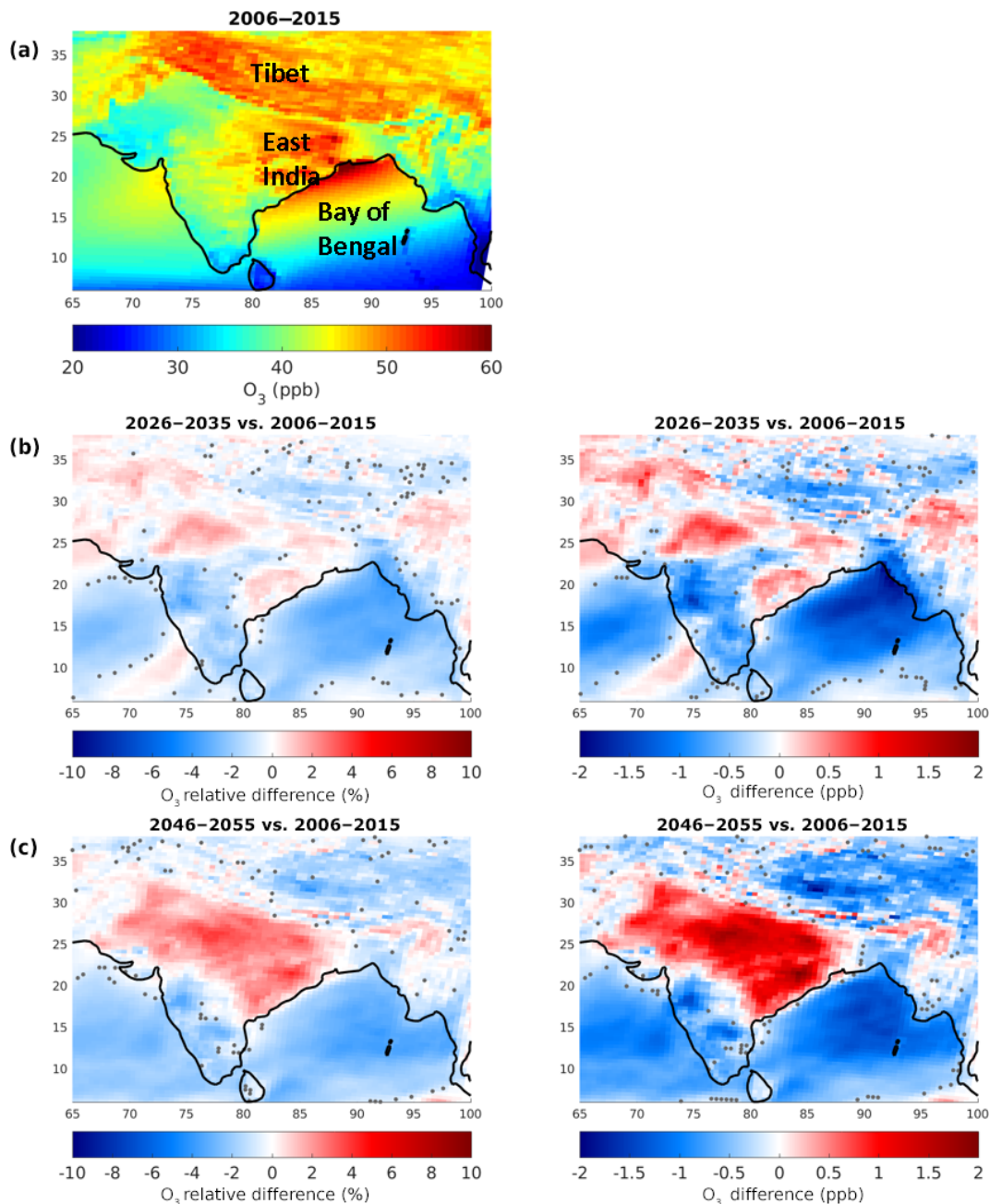


Figure 7. (a) Distribution of surface O₃ mixing ratios (in ppb) for the reference scenario. Distribution of the relative difference and absolute difference in surface O₃ between the reference scenario and the FC2030 scenario (b) and the FC2050 scenario (c). The relative differences are calculated as $([\text{FC} - \text{reference}] / \text{reference}) \times 100\%$, and the absolute differences as $[\text{FC} - \text{reference}]$. Grey dots mark grid points that do not satisfy the 95 % level of significance.

distribution of the relative differences. For these regions, the deposition velocity is correlated with the surface O₃, in contrast to the anti-correlation found over the rest of the domain.

During the pre-monsoon period, region (A) is characterized by a high level of NMVOCs and NO_x. During the winter, the regions (B) and (C) are characterized by a high level of NMVOCs and a low level of NO_x (Fig. S8).

During the pre-monsoon period, a decrease in NO_x and NMVOC is simulated over region (A) (Fig. S8). The reduction of these two precursors may explain the decrease in O₃. The two other regions, regions (B) and (C), are both characterized during winter by a decrease in NO_x and an increase in NMVOCs. Combined with the increase in O₃, this result gives an indication of the presence of a VOC-sensitive

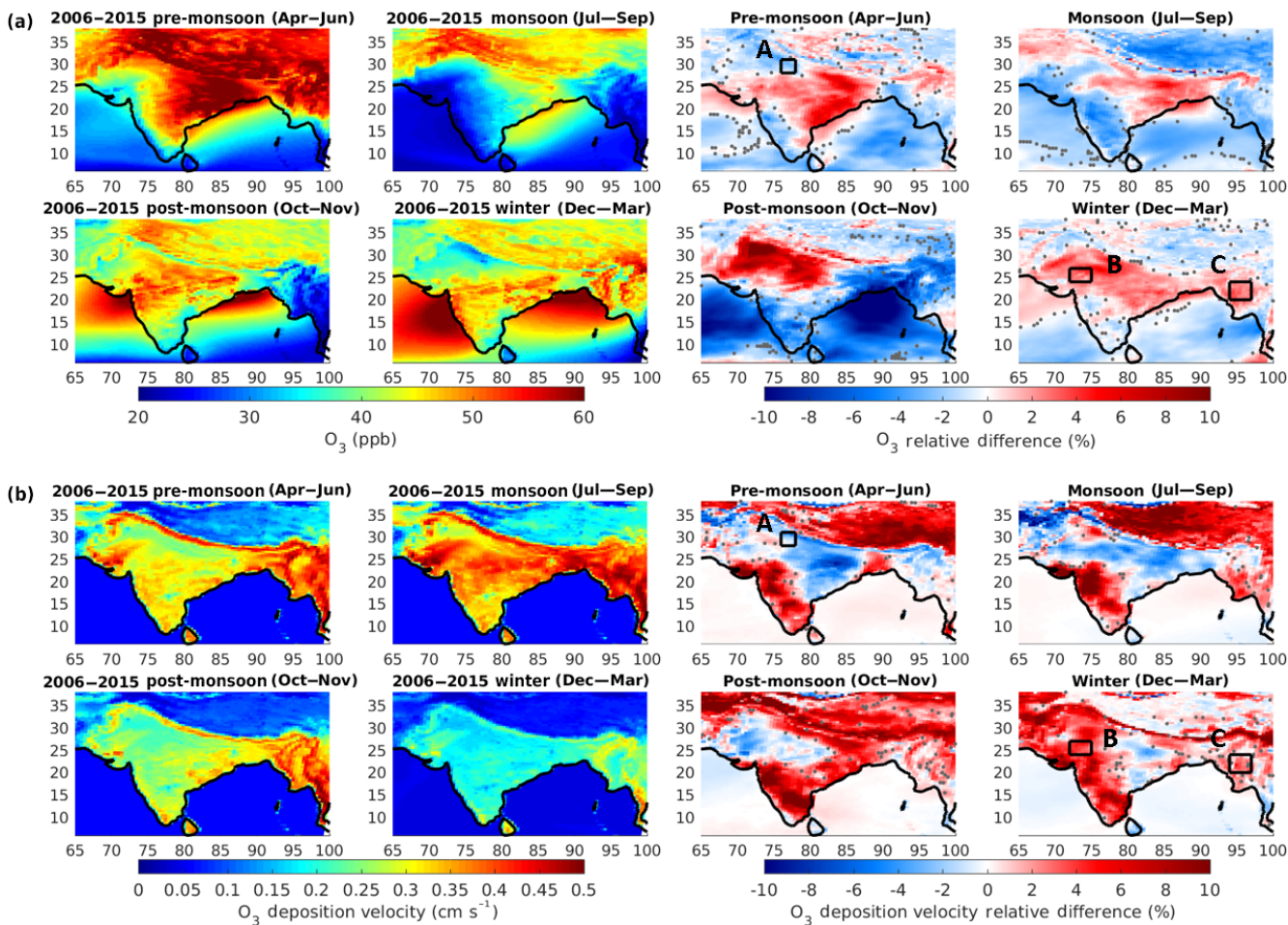


Figure 8. (a) Seasonal distribution of O₃ and relative difference between the reference scenario and the FC2050 scenario. (b) Seasonal distribution of O₃ deposition velocity and relative difference between the reference scenario and the FC2050 scenario. The relative differences are calculated as $([\text{FC2050} - \text{reference}] / \text{reference}) \times 100\%$. Regions discussed in the text are noted on the distributions of relative difference. Grey dots mark grid points that do not satisfy the 95 % level of significance.

regime. This contrasts with the NO_x-sensitive regime otherwise prevailing in India as calculated by Sharma et al. (2016) and observed by Mahajan et al. (2015). It is however interesting to note that the presence of a VOC-limited regime over region (A) during the pre-monsoon period and over region (B) in winter, was already observed by satellite measurements (Mahajan et al., 2015).

The NMVOCs for the reference scenario over region (C), corresponding mainly to Myanmar, are probably from biomass burning as the peak forest fire season in this region occurs in winter (e.g. van der Werf et al., 2010 or Pommier et al., 2017).

For the FC2030 scenario, an identical pattern is observed with an anti-correlation between the relative difference in O₃ and the relative difference in V_d(O₃), also with the exception of three other regions (A', B' and C') as shown in Fig. S7. This shows that the change in O₃ is related to the change in V_d(O₃), except over three regions, as for the FC2050 sce-

nario. Over these three regions, the complementary effect of NO_x-NMVOCs is also obvious in this scenario (Fig. S9). The change in location of the three regions between the 2030s and the 2050s shows that the local meteorology has an impact on the change in the chemistry, such as the surface temperature. Indeed, the changes in temperature are not homogeneous over the domain and vary with the seasons.

4.2 PM_{2.5}

In the reference scenario, the largest surface PM_{2.5} concentrations are located over the Indo-Gangetic Plain (Fig. 9), known to be a highly populated area (e.g. Chowdhury and Maithani 2014; or <http://www.census2011.co.in/states.php>) and as a large source of pollutants emissions (e.g. Clarisse et al., 2009; Mallik and Lal, 2014; Tiwari et al., 2016).

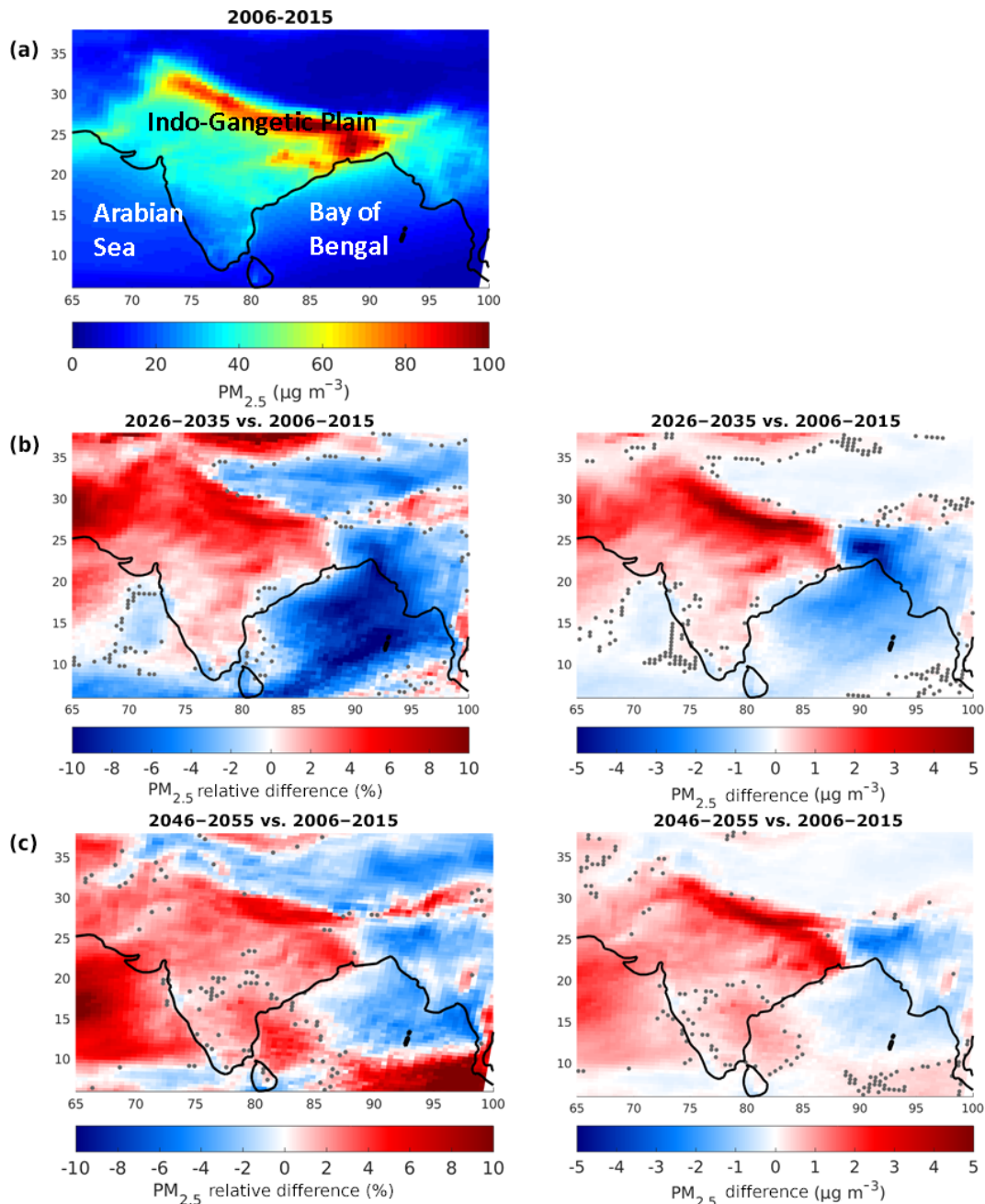


Figure 9. (a) Distribution of surface PM_{2.5} concentrations (in $\mu\text{g m}^{-3}$) for the reference scenario. Distribution of the relative difference and absolute difference in surface PM_{2.5} concentrations between the reference scenario and the FC2030 scenario (b) and the FC2050 scenario (c). The relative differences are calculated as $([\text{FC} - \text{reference}] / \text{reference}) \times 100\%$, and the absolute differences as $[\text{FC} - \text{reference}]$. Grey dots mark grid points that do not satisfy the 95 % level of significance.

According to these calculations, climate change has a larger impact, in terms of absolute values, on PM_{2.5} than on O₃. Climate change is predicted to lead a fairly homogeneous rise in surface PM_{2.5} levels over India, especially for the FC2050 scenario, by up to 6.5 % (4.6 $\mu\text{g m}^{-3}$) (Fig. 9). This maximum increase is located over the Indo-Gangetic Plain, where a decrease in surface wind speed is predicted

(not shown). The decrease in wind speed may limit the emission of dust and the dispersion of the PM_{2.5} emitted over this area. In both FC scenarios, an increase in surface PM_{2.5} concentrations is predicted for the western part of the domain (Arabian Sea) and a decrease over the eastern part of the domain (Bay of Bengal). It is worth noting that with a mesoscale model, Glotfelty et al. (2016) also simulated an

increase in PM_{2.5} over India. However, a proper comparison with other studies remains difficult, as different models or scenarios were used. It is also noteworthy that the changes in PM_{2.5} are statistically significant at the 95 % confidence level.

The distribution of the relative difference in PM_{2.5} is roughly homogeneous in the FC2050 scenario over India (Fig. 9) but it does not match the pattern of precipitation change (Fig. S10). As PM_{2.5} is highly sensitive to wet scavenging, we would expect an impact of changes in precipitation on the change in PM_{2.5}, but this relationship is not shown in these distributions (Figs. 9 and S10).

The composition of PM_{2.5} is mainly dominated by dust, OM and secondary inorganic aerosol (SIA). SIA includes SO₄²⁻, NO₃⁻ and NH₄⁺. The seasonal distribution of their contribution on PM_{2.5} provides complementary information on the composition of PM_{2.5} (Fig. S11). Generally speaking, dust dominates during the pre-monsoon and monsoon periods over India, while the amounts of OM and SIA are large during the post-monsoon period and in winter. It is also worth noting that PM_{2.5} over the Arabian Sea and Tibet are mostly influenced by dust for each season. Dust over the Arabian Sea originates from the Sahara Desert, while the Tibet Plateau is a known regional source of dust (e.g. Xu et al., 2015; Xin et al., 2016). PM_{2.5} over the Bay of Bengal is largely impacted by dust during the monsoon and OM during the winter.

The simulated OM is mainly composed of SOA. It is also interesting to note that the OM over Myanmar (region C in Fig. 8) is strongly influenced by primary emissions from fires and spatially coincides with the O₃ production seen previously in Fig. 8. SOA is predicted to increase, by up to 19 % for FC2030 and up to 33 % for FC2050 over India. This rise is probably due to an increase in biogenic VOCs as suggested by Heald et al. (2008) (see also Fig. S8b) as a result of temperature increases. As noted above though, isoprene emissions might actually be inhibited by CO₂ effects in a future climate, and neither Heald's model nor ours accounts for such effects.

In order to better interpret the seasonal process, more detailed examples over India for the FC2050 scenarios with three regions are shown in Fig. 10. The results with the FC2030 scenario (not shown) lead to similar conclusions. The composition of PM_{2.5} over these regions coincides with the overall description provided by Fig. S11, i.e. there is a large amount of dust during the pre-monsoon and the monsoon; and OM and SIA during the post-monsoon and the winter. Wind speed is also higher during the pre-monsoon and the monsoon for these three regions, explaining the large amount of dust during these seasons. The budget of dust is sensitive to precipitation, while OM and SIA are also highly related to chemistry, as described hereafter.

Indeed, region (1), representing mainly a rural area, is subject to a large decrease in PM_{2.5} by 8 % during the monsoon. This is mainly due to the reduction in dust, representing 55 % of PM_{2.5}, largely scavenged by the increased precipitation

(+36 %) (as explained in Section 2.1). The increase in PM_{2.5} during the pre-monsoon and during the winter is linked to the increase in dust by 15 % and in OM by 10 %, respectively. This increase in dust depends on the change in precipitation (10 % decrease) and probably also on the increase in wind speed by 3 %. The augmentation in OM is related to the increase in biogenic emissions as isoprene (+14 %) and monoterpene (+11 %). During the post-monsoon, the slight rise in PM_{2.5} is mainly due to the increase in OM and SIA.

The impact of dust is also still high for a region located far from the desert as region (2), but the change in the PM_{2.5} level is also largely related to the change in SIA and OM in all seasons. Region (2) experiences a larger change in PM_{2.5} during the monsoon (-5 %) related to the increased precipitation (+35 %) and the post-monsoon (+7 %), probably linked to the increase in isoprene and in monoterpene emissions (+13 % and +11 %, respectively). The reduction in precipitation by 25 % during the pre-monsoon probably explains the increase in PM_{2.5}.

For region (3), located within the Indo-Gangetic Plain and which includes Delhi, the largest variation in PM_{2.5} by 20 % is modelled during the post-monsoon. This shows that this region is affected by a large penalty from the climate change on surface PM_{2.5} concentrations during the post-monsoon. This increase is caused by the rise in both SIA (+29 %) and OM (+21 %) and probably by the reduction of the dispersion as predicted by the decrease in the surface wind speed by 5 %. The augmentation in SIA and OM may be related to the large increase in isoprene and in monoterpene emissions (+19 % both), explained by increased temperature. Among all the seasons and among the three selected regions, the larger increase in temperature (+0.6 %) occurs in this case. It is also worth noting that it coincides with the larger growth in O₃ among these three regions (+6 %). The changes during the pre-monsoon and the winter are mainly due to the variation in SIA, and the joint changes in SIA and OM, respectively. The decrease in PM_{2.5} during the monsoon is linked to the reduction in dust and in SIA (by 5 % for both), which are linked to the increase in precipitation (+16 %) over this wet region (2.8 mm day⁻¹).

In addition to confirming the seasonal variation in the composition of PM_{2.5} over India as shown in Fig. S11, these three cases show that the main parameters influencing the changes in the main components (SIA, OM and dust), are the precipitation, the biogenic emissions and the wind speed.

5 Impact of future emission scenarios combined with climate change

By combining the climate effect with future changes in emissions, we explore the differences between the FCE scenarios (2030 and 2050) and the reference scenario. As in the previous sections, the simulated fields were averaged over their respective period of simulation.

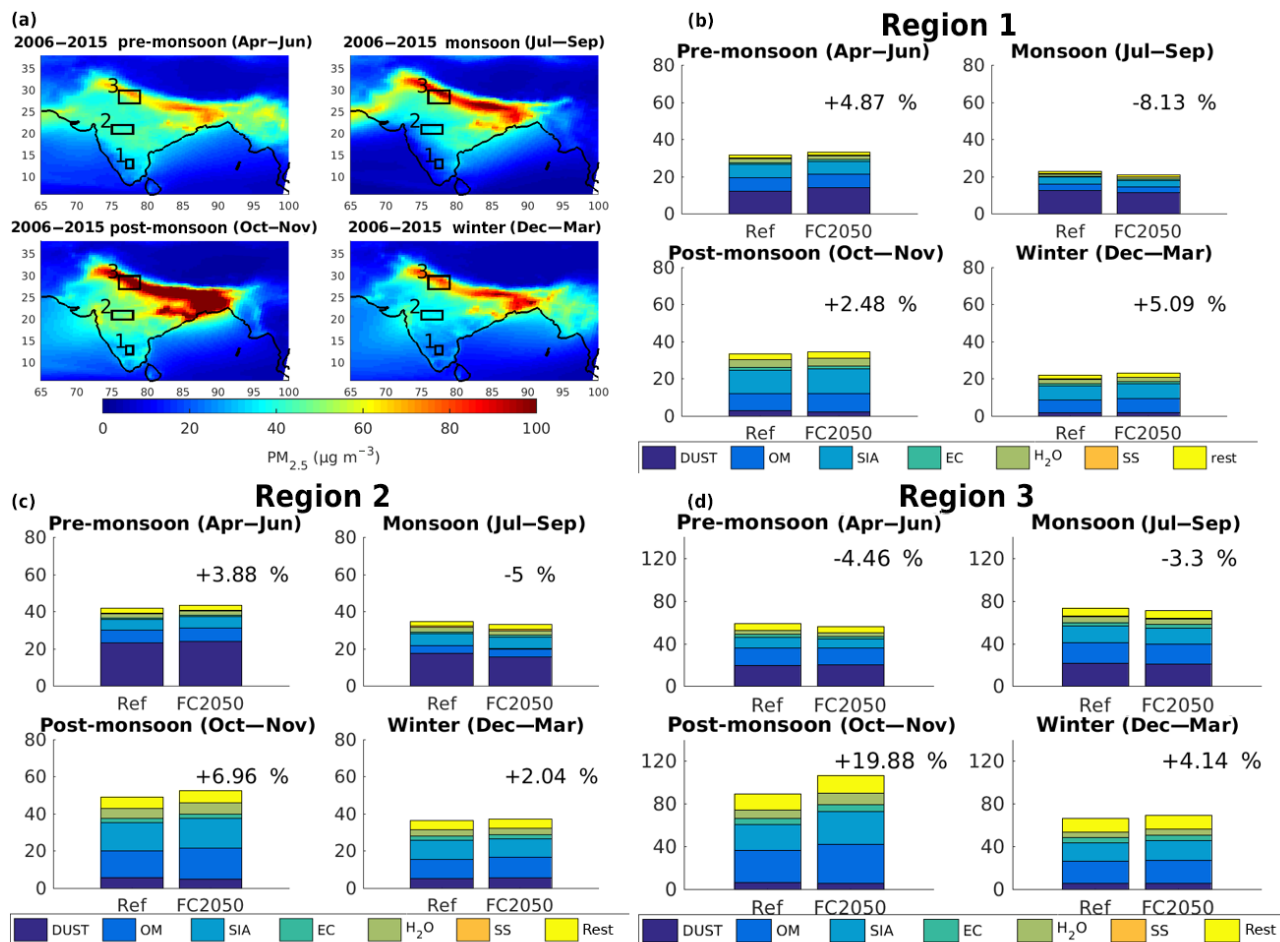


Figure 10. Seasonal distribution of surface PM_{2.5} concentrations (in $\mu\text{g m}^{-3}$) for the reference scenario, and seasonal composition of PM_{2.5} (in $\mu\text{g m}^{-3}$) for the three regions highlighted by black boxes on the map for the reference and the FC2050 scenarios. The black percent corresponds to the relative difference in PM_{2.5} between both scenarios for each region. Note the different y axis for Region 3.

5.1 O₃

For both FCE scenarios, a substantial increase in O₃ over India is modelled, as shown in Fig. 11. This augmentation in O₃ reaches 13 % or 5 ppb in the 2030s (mean of 3 % or 1 ppb) and reaching 45 % or 18 ppb in the 2050s (mean of 13 % or 6 ppb) within the domain defined by the black box in Fig. 11 (latitudes 8–38° N and the longitudes 68–90° E). The increase in O₃ is noticeable during the four seasons but it is more intense during the monsoon as shown by Fig. 12. It is worth noting that there is a decrease in O₃ over the Western Ghats during the monsoon – e.g. region α in Fig. 12: –12 % in 2030 (not shown) and –4 % in 2050 – while the rise in O₃ over the rest of the country is larger than for the other seasons. This contrast between the Western Ghats and the rest of India is more pronounced in the FCE2030 scenario. Another region (labelled as β) in winter, is also characterized by a decrease in O₃ – 11 % in 2030 (not shown), –4 % in 2050 (Fig. 12). Both reductions can be explained by

the NO_x–VOC chemistry. Both precursors largely increase in the FCE2030 and FCE2050 scenarios as shown by the large relative differences presented in Fig. S12. However, regions (α) and (β) present a decrease in their NMVOC / NO_x ratio in the future (Fig. S12). This ratio is already lower in the reference scenario for both regions (≤ 16 , Fig. S12) than in the rest of India since the mean ratio over land covering the area defined in Fig. 11 is close to 60. This means that NO_x increases more for these regions than NMVOC, probably developing a NO_x-saturated regime and causing the O₃ depletion. Thus both regions, for their respective season, suggest a VOC-sensitive regime for the FCE2030 and FCE2050 scenarios.

This substantial increase in O₃ leads to a large increase in the ozone health indicator, SOMO35. The SOMO35 metric is defined as the annual sum of daily maximum running 8 h average O₃ concentrations over 35 ppb. The SOMO35 levels for the reference scenario are already higher (Fig. S13) than over Europe (e.g. van Loon et al., 2007; EMEP Status Re-

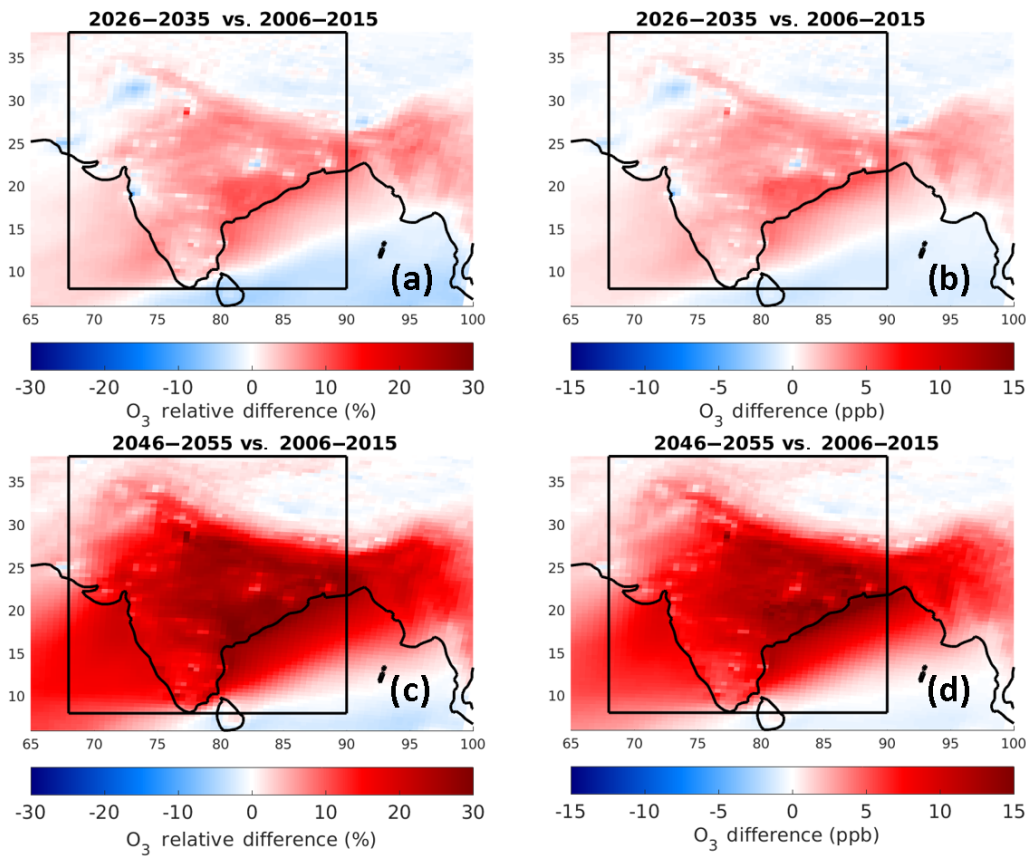


Figure 11. Distribution of the relative difference (**a, c**) and absolute difference (**b, d**) in surface O₃ between the reference and the FCE2030 scenario (**a–b**) and the FCE2050 scenario (**c–d**). The relative differences are calculated as $([\text{FCE} - \text{reference}] / \text{reference}) \times 100\%$, and the absolute differences as $[\text{FCE} - \text{reference}]$. The black box delimits the region described in the text.

port 1/2017), probably related to the warmer climate and the large emissions of O₃ precursors over India, and the overestimation in O₃ from the model as shown in Sect. 3.1. SOMO35 is predicted to significantly increase for both FCE scenarios (Fig. S13).

5.2 PM_{2.5}

Climate change has a non-negligible impact on surface PM_{2.5} concentrations, but this impact is small compared with the effects of emissions in the FCE scenarios. Looking at the PM_{2.5} in Fig. 13, a large increase is simulated throughout the domain. This rise in surface concentrations is larger in the FCE2050 scenario than in the FCE2030 scenario. Within the region delimited by the black box in Fig. 13 (same as Fig. 11), the mean rise in PM_{2.5} is equal to 37 % (13 µg m⁻³) in the 2030s and to 67 % (23 µg m⁻³) in the 2050s. These increments alone are comparable to the annual threshold that WHO recommends not to exceed, i.e. 10 µg m⁻³, for the FCE2030 scenario, and double that for the FCE2050 scenario. This increase in concentrations is also large for each season (Fig. S14). It has a maximum during the post-monsoon in both scenarios, reaching 117 % (119 µg m⁻³) in

the 2030s (not shown) and 172 % (168 µg m⁻³) in the 2050s. These huge numbers prefigure an enormous increase in fine particulate matter over India, as already suggested by Amann et al. (2017), and imply serious health issues for the population, especially children (UNICEF, 2016).

As expected by the large increase in emissions as for SO_x and NO_x presented in Fig. 1, the future concentrations of PM_{2.5} are influenced by SO₄²⁻, NO₃⁻ and NH₄⁺ for each season. These compounds also show the largest increase during the post-monsoon season. This is particularly obvious for the three selected regions of Fig. 10 since SIA increases by at least 100 % in the FCE2030 scenario and by at least 200 % in the FCE2050 scenario (Fig. S15). The larger increase in PM_{2.5} is simulated over region (2) for both FCE scenarios during the post-monsoon; by 75 % in the 2030s and 132 % in the 2050s (Fig. S15). Region (3), characterized by the large impact of climate on its PM_{2.5} during the post-monsoon as shown previously in Fig. 10, has an increase in PM_{2.5} by around 69 % in FCE2030 and 112 % in FCE2050.

While the surface PM_{2.5} over the land region delimited in Fig. 13 is composed on average by 5.1 % of NH₄⁺, 6.8 % of NO₃⁻, and 9.7 % of SO₄²⁻ for the reference scenario; their

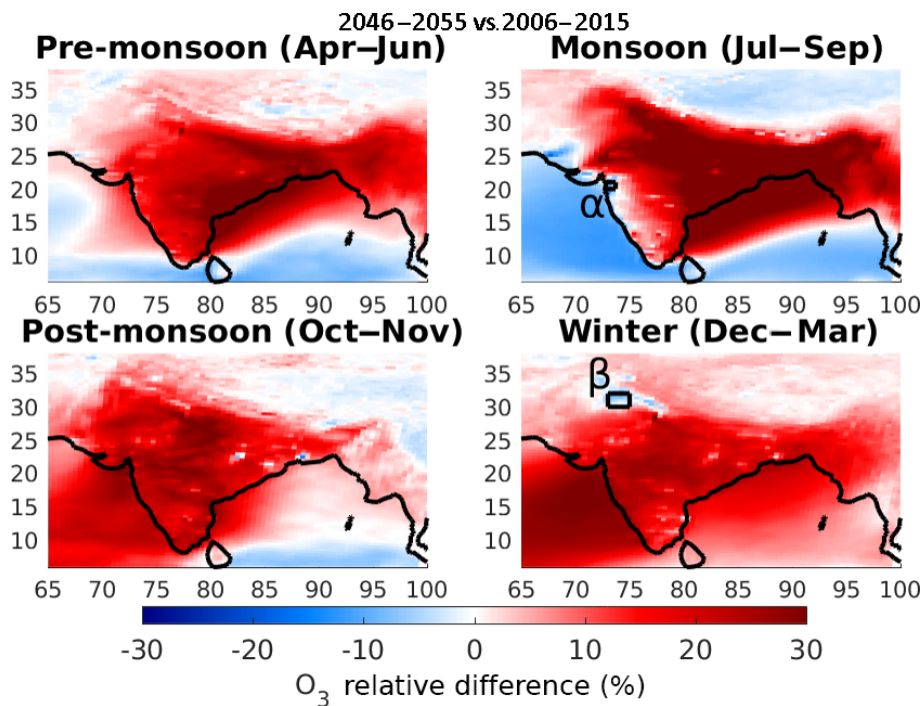


Figure 12. Seasonal distribution of the relative difference in surface O_3 between the reference scenario and the FCE2050 scenario. The relative differences are calculated as $([FCE2050 - \text{reference}] / \text{reference}) \times 100\%$. Regions discussed in the text are noted on the distributions for their respective season.

mean contribution grows and becomes respectively 6.7, 7.2 and 13.6 % in the 2030s and 7.8, 7.5 and 16.8 % in the 2050s. OM and the dust remain two major components of surface $PM_{2.5}$ but in the 2030s, SIA becomes the second largest component since it represents 28 % of $PM_{2.5}$ (29 % for dust and 19 % for OM) and the main component in the 2050s with 32 %, while dust represents 25 % and OM corresponds to 18 % of $PM_{2.5}$. It is also worth noting that even though the PPM are high for the three scenarios (close to 20 % of $PM_{2.5}$), the amount of EC within these PPM remains low, around 15 %.

It is interesting to note that even under increasing anthropogenic emissions a significant fraction of $PM_{2.5}$ comes from sources (dust and some fraction of SOA) that are challenging to control through policy measures. Still, even biogenic SOA is partly the product of anthropogenic emissions (and certainly land-use policy, e.g. Tsigaridis and Kanakidou, 2007; Ashworth et al., 2012), and dust is also partly a function of land-use and climate change. But such interactions are beyond the scope of our study.

6 Conclusions

Driven by downscaled meteorological fields, the EMEP model was applied to investigate the impact of changes in regional climate and emissions on surface O_3 and $PM_{2.5}$ over India. The evaluation of the reference scenario with surface-

based observations suggests a fair simulation of the seasonal variation of O_3 and a good representation of surface $PM_{2.5}$ concentrations over Indian cities. Additional information on the chemical components in $PM_{2.5}$ will be helpful to interpret the differences and confirm the large part of primary organic matter simulated in winter by EMEP and the high ratio of dust during the monsoon. EMEP overestimates O_3 by 11 ppb and we suspect that NO_x titration over cities, unresolved by a rather coarse grid (ca. 50 km), and possibly uncertainties in the emissions, are the main cause, especially in winter. However, there is a lack of reliable available measurements of NO_x and O_3 to fully validate this assumption.

The O_3 change due to regional climate change for the medium-term (FC2050) scenario highlights a clear north-south gradient over India, with an increase over the north, by up to 4.4 % (2 ppb) and a decrease over the south, by up to -3.4% (-1.4 ppb). This O_3 budget is highly impacted by the change in O_3 deposition velocity due to the change in soil moisture, and over a few areas by the biogenic NMVOCs. Climate change leads to increases in the $PM_{2.5}$ levels at short and medium-terms, reaching a maximum of 6.5 % ($4.6 \mu g m^{-3}$) over the Indo-Gangetic Plain by the 2050s. The $PM_{2.5}$, mainly composed of dust, OM and SIA, is mainly controlled by change in precipitation and biogenic emissions. For example, over the Indo-Gangetic Plain, an increase of 20 % during the post-monsoon is predicted, related to a rise in isoprene and in monoterpene emissions, while a rural re-

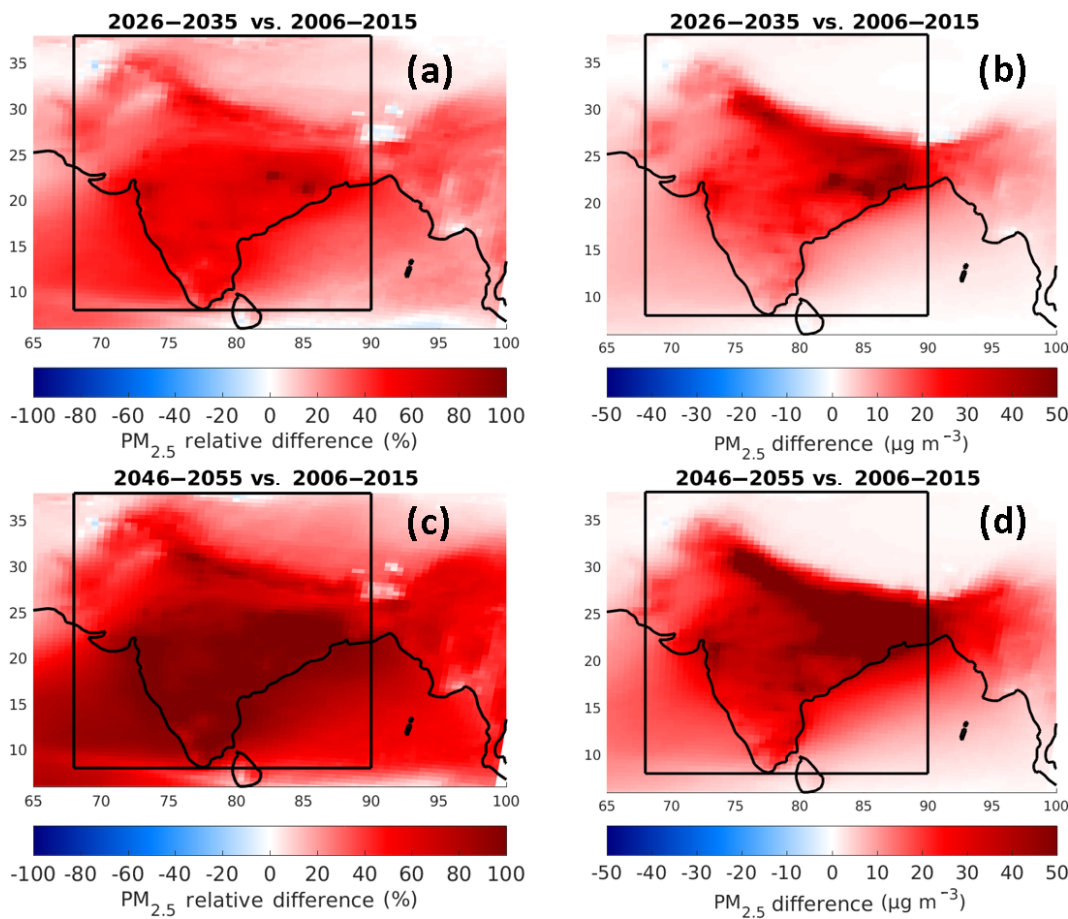


Figure 13. Distribution of the relative difference (**a, c**) and absolute difference (**b, d**) in surface PM_{2.5} between the reference scenario and the FCE2030 scenario (**a–b**) and the FCE2050 scenario (**c–d**). The relative differences are calculated as $([\text{FCE} - \text{reference}] / \text{reference}) \times 100\%$, and the absolute differences as $[\text{FCE} - \text{reference}]$. The black box delimits the region described in the text.

gion is characterized by a 8 % decrease in PM_{2.5} during the monsoon, linked to the increased precipitation in 2050.

A large increase in anthropogenic emissions is predicted if no further policy efforts are made. Combined with climate change impacts; these emissions are predicted to lead to large changes in surface O₃ and PM_{2.5}. For surface O₃, these changes reach 45 % over some regions in 2050. This augmentation is substantial for each season, with the exception of two regions – as e.g. over the Western Ghats during the monsoon characterized a decrease in O₃ around -12 % in 2030 (-4 % in 2050) related to the dependence of O₃ production on the NO_x and VOC concentrations.

India is predicted to suffer large increases in PM_{2.5} levels due to the increases in anthropogenic emissions in this no-further control scenario. The increase in PM_{2.5} will occur rapidly since the mean rise is close to 37 % for the short-term scenario (2030s) and 67 % for the medium-term scenario (2050s) over the main part of the country. The PM_{2.5} levels are predicted to reach very high levels, up to a maximum of 117 % (119 µg m⁻³) increase in the 2030s and 172 %

(168 µg m⁻³) in the 2050s during the post-monsoon season. In the 2030s, the SIA will become the second largest component of PM_{2.5} over India, exceeding the amount of OM by reaching a ratio close to 28 % and the main component in the 2050s with 32 %.

Finally, we note that this is the first serious attempt to use the EMEP model over the Indian subcontinent, and there are likely many improvements needed before modelling skill achieves the same level as obtained in European simulations. For example, the vegetation characterization used in the EMEP model was focused on European vegetation, and is probably not fully suitable for India, which may affect the response in temperature over India. Many issues affect any modelling study for this region. For example, emission rates of biogenic VOC from vegetation over India are also largely unknown; Guenther et al. (2006) show only one site in or near the Himalayas – and nothing over the rest of the Indian sub-continent. Emissions of other compounds are also rather uncertain. Proper model evaluation in this region would require quality-assured measurements of a range of compounds

in rural as well as urban areas. Still, given the rapidly increasing emission and pollution levels in India, it is clear that further efforts are warranted, and increasing attention will improve the basis for future model verification and hence for a sounder basis for emissions policy assessments in future.

Data availability. The EMEP model is an open-source model available at <https://github.com/metno/emep-ctm> (Simpson et al., 2012).

Appendix A

Table A1. Error statistics used to evaluate the model performance (M and O refer, respectively, to model and observation data, and N is the number of observations).

Validation metrics	Formula	Range	Ideal score
Mean bias (MB) ^a	$\frac{\sum_{i=1}^N (M_i - O_i)}{N}$	−∞ to +∞	0
Normalized mean bias (NMB) ^b	$\frac{\sum_{i=1}^N (M_i - O_i)}{\sum_{i=1}^N O_i} \times 100\%$	0 to +∞	0
Mean normalized gross error (MNGE) ^c	$\frac{1}{N} \sum_{i=1}^N \frac{ M_i - O_i }{O_i} \times 100\%$	0 to +∞	0
Root mean square error (RMSE) ^d	$\sqrt{\frac{\sum_{i=1}^N (M_i - O_i)^2}{N}}$	0 to +∞	0

^a The MB provides the information about the absolute bias of the model, with negative values indicating underestimation and positive values indicating overestimation by the model. ^b The NMB represents the model bias relative to observations. ^c The MNGE represents mean absolute difference between model and observations relative to the observations. ^d The RMSE considers error compensation due to opposite sign differences and encapsulates the average error produced by the model.

The Supplement related to this article is available online at <https://doi.org/10.5194/acp-18-103-2018-supplement>.

Competing interests. The authors declare that they have no conflict of interest.

Acknowledgements. The work related to climate modelling has been supported by the Research Council of Norway through the CLIMATRANS project (grant 235559) as well as NOTUR project “EMEP” (nn2890k) and NorStore project “European Monitoring and Evaluation Programme” (ns9005k). The EMEP project itself is supported by the Convention on the Long Range Transmission of Air Pollutants, under UN-ECE.

Edited by: Qiang Zhang

Reviewed by: three anonymous referees

References

- Ainsworth, E. A., Yendrek, C. R., Sitch, S., Collins, W. J., and Emberson, L. D.: The Effects of Tropospheric Ozone on Net Primary Productivity and Implications for Climate Change, *Ann. Rev. Plant Biol.*, 63, 637–661, 2012.
- Amann, M., Bertok, I., Borken-Kleefeld, J., Cofala, J., Heyes, C., Höglund-Isaksson, L., Klimont, Z., Nguyen, B., Posch, M., Rafaj, P., Sandler, R., Schöpp, W., Wagner, F., and Winiwarter, W.: Cost-effective control of air quality and greenhouse gases in Europe: Modeling and policy applications, *Environ. Model. Softw.*, 26, 1489–1501, <https://doi.org/10.1016/j.envsoft.2011.07.012>, 2011.
- Amann, M., Klimont, Z., and Wagner, F.: Regional and Global Emissions of Air Pollutants: Recent Trends and Future Scenarios, *Annu. Rev. Env. Resour.*, 38, 31–55, <https://doi.org/10.1146/annurev-environ-052912-173303>, 2013.
- Amann, M., Purohit, P., Bhanarkar, A. D., Bertok, I., Borken-Kleefeld, J., Cofala, J., Heyes, C., Kiesewetter, G., Klimont, Z., Liu, J., Majumdar, D., Nguyen, B., Rafaj, P., Rao, P. S., Sander, R., Schöpp, W., Srivastava, A., and Vardhan, B. H.: Managing future air quality in megacities: A case study for Delhi, *Atmos. Environ.*, <https://doi.org/10.1016/j.atmosenv.2017.04.041>, 2017.
- Arneth, A., Miller, P. A., Scholze, M., Hickler, T., Schurgers, G., Smith, B., and Prentice, I. C.: CO₂ inhibition of global terrestrial isoprene emissions: Potential implications for atmospheric chemistry, *Geophys. Res. Lett.*, 34, L18813, <https://doi.org/10.1029/2007GL030615>, 2007.
- Ashworth, K., Folberth, G., Hewitt, C. N., and Wild, O.: Impacts of near-future cultivation of biofuel feedstocks on atmospheric composition and local air quality, *Atmos. Chem. Phys.*, 12, 919–939, <https://doi.org/10.5194/acp-12-919-2012>, 2012.
- Atkinson, R. W., Cohen, A., Mehta, S., and Anderson, H. R.: Systematic Review and Meta-Analysis of Epidemiological Time-Series Studies on Outdoor Air Pollution and Health In Asia, *Air Qual. Atmos. Hlth.*, 5, 383–391, <https://doi.org/10.1007/s11869-010-0123-2>, 2012.
- Bentsen, M., Bethke, I., Debernard, J. B., Iversen, T., Kirkevåg, A., Seland, Ø., Drange, H., Roelandt, C., Seierstad, I. A., Hoose, C., and Kristjánsson, J. E.: The Norwegian Earth System Model, *NorESM1-M – Part 1: Description and basic evaluation of the physical climate*, *Geosci. Model Dev.*, 6, 687–720, <https://doi.org/10.5194/gmd-6-687-2013>, 2013.
- Bergström, R., Denier van der Gon, H. A. C., Prévôt, A. S. H., Yttri, K. E., and Simpson, D.: Modelling of organic aerosols over Europe (2002–2007) using a volatility basis set (VBS) framework: application of different assumptions regarding the formation of secondary organic aerosol, *Atmos. Chem. Phys.*, 12, 8499–8527, <https://doi.org/10.5194/acp-12-8499-2012>, 2012.
- Brauer, M., Freedman, G., Frostad, J., van Donkelaar, A., Martin, R. V., Dentener, F., van Dingenen, R., Estep, K., Amini, H., Apte, J. S., Balakrishnan, K., Barregard, L., Broday, D., Feigin, V., Ghosh, S., Hopke, P. K., Knibbs, L. D., Kokubo, Y., Liu, Y., Ma, S. F., Morawska, L., Sangrador, J. L. T., Shaddick, G., Anderson, H. R., Vos, T., Forouzanfar, M. H., Burnett, R. T., and Cohen, A.: Ambient Air Pollution Exposure Estimation for the Global Burden of Disease 2013, *Env. Sci. Technol.*, 50, 79–88, <https://doi.org/10.1021/acs.est.5b03709>, 2016.
- Büker, P., Morrissey, T., Briolat, A., Falk, R., Simpson, D., Tuovinen, J.-P., Alonso, R., Barth, S., Baumgarten, M., Grulke, N., Karlsson, P. E., King, J., Lagergren, F., Matyssek, R., Nunn, A., Ogaya, R., Peñuelas, J., Rhea, L., Schaub, M., Uddling, J., Werner, W., and Emberson, L. D.: DO3SE modelling of soil moisture to determine ozone flux to forest trees, *Atmos. Chem. Phys.*, 12, 5537–5562, <https://doi.org/10.5194/acp-12-5537-2012>, 2012.
- Callaghan, A., de Leeuw, G., Cohen, L., and O'Dowd, C. D.: Relationship of oceanic whitecap coverage to wind speed and wind history, *Geophys. Res. Lett.*, 35, L23609, <https://doi.org/10.1029/2008GL036165>, 2008.
- Chatani, S., Amann, M., Goel, A., Hao, J., Klimont, Z., Kumar, A., Mishra, A., Sharma, S., Wang, S. X., Wang, Y. X., and Zhao, B.: Photochemical roles of rapid economic growth and potential abatement strategies on tropospheric ozone over South and East Asia in 2030, *Atmos. Chem. Phys.*, 14, 9259–9277, <https://doi.org/10.5194/acp-14-9259-2014>, 2014.
- Chowdhury, P. K. R. and Maithani, S.: Modelling urban growth in the Indo-Gangetic plain using nighttime OLS data and cellular automata, *Int. J. Appl. Earth Obs.*, 33, 55–165, <https://doi.org/10.1016/j.jag.2014.04.009>, 2014.
- Clarisse, L., Clerbaux, C., Dentener, F., Hurtmans, D., and Coheur, P.-F.: Global ammonia distribution derived from infrared satellite observations, *Nat. Geosci.*, 2, 479–483, <https://doi.org/10.1038/ngeo551>, 2009.
- Cooper, O. R., Parrish, D. D., Ziemke, J., Balashov, N. V., Cupeiro, M., Galbally, I. E., Gilge, S., Horowitz, L., Jensen, N. R., Lamarque, J.-F., Naik, V., Oltmans, S. J., Schwab, J., Shindell, D. T., Thompson, A. M., Thouret, V., Wang, Y., and Zbinden, R. M.: Global distribution and trends of tropospheric ozone: An observation-based review, *Elem. Sci. Anth.*, 2, 29, <https://doi.org/10.12952/journal.elementa.000029>, 2014.
- Crutzen, P. J., Lawrence, M. G., and Pöschl, U.: On the background photochemistry of tropospheric ozone, *Tellus A*, 51, 123–146, 1999.

- Dash, S. K., Jenamani, R. K., Kalsi, S. R., and Panda, S. K.: Some evidence of climate change in twentieth-century India, *Climatic Change*, 85, 299–321, 2007.
- Dey, S., Di Girolamo, L., van Donkelaar, A., Tripathi, S. N., Gupta, T., and Mohan, M.: Variability of outdoor fine particulate ($PM_{2.5}$) concentration in the Indian Subcontinent: A remote sensing approach, *Remote Sens. Environ.*, 127, 153–161, <https://doi.org/10.1016/j.rse.2012.08.021>, 2012.
- Emberson, L., Simpson, D., Tuovinen, J.-P., Ashmore, M., and Cambridge, H.: Towards a model of ozone deposition and stomatal uptake over Europe, The Norwegian Meteorological Institute, Oslo, Norway, 2000.
- Emberson, L., Ashmore, M., Simpson, D., Tuovinen, J.-P., Cambridge, H.: Modelling and mapping ozone deposition in Europe, *Water Air Soil Pollut.*, 130, 577–582, 2001.
- Emberson, L. D., Büker, P., and Ashmore, M. R.: Assessing the risk caused by ground level ozone to European forest trees: A case study in pine, beech and oak across different climate regions, *Environ. Pollut.*, 147, 454–466, 2007.
- EMEP Status Report 1/2015: “Transboundary particulate matter, photo-oxidants, acidifying and eutrophying components”, Joint MSC-W & CCC & CEIP Report, ISSN 1504-6109, 2015.
- EMEP Status Report 1/2017: “Transboundary particulate matter, photo-oxidants, acidifying and eutrophying components”, Joint MSC-W & CCC & CEIP Report, 15–36, ISSN 1504-6109, 2017.
- Engardt, M.: Modelling of near-surface ozone over South Asia, *J. Atmos. Chem.*, 59, 61–80, <https://doi.org/10.1007/s10874-008-9096-z>, 2008.
- Fann, N., Lamson A. D., Anenberg, S. C., Wesson, K., Risley D., and Hubbell, B. J.: Estimating the national public health burden associated with exposure to ambient $PM_{2.5}$ and ozone, *Risk Anal.*, 32, 81–95, 2012.
- Fiore, A., Naik, V., and Leibensperger, E. M.: Air Quality and Climate Connections, *JAPCA J. Air Waste Ma.*, 6, 645–685, <https://doi.org/10.1080/10962247.2015.1040526>, 2015.
- Forouzanfar, M. H., Alexander, L., Anderson, H. R., Bachman, V. F., and Biryukov, S.: Global, regional, and national comparative risk assessment of 79 behavioural, environmental and occupational, and metabolic risks or clusters of risks in 188 countries, 1990–2013: a systematic analysis for the Global Burden of Disease Study 2013, 386, 2287–2323, 2015.
- Ganzeveld, L., Helmig, D., Fairall, C. W., Hare, J., and Pozzer, A.: Atmosphere-ocean ozone exchange: A global modeling study of biogeochemical, atmospheric, and waterside turbulence dependencies, *Global Biogeochem. Cy.*, 23, GB4021, <https://doi.org/10.1029/2008GB003301>, 2009.
- Gerber, H. E.: Relative-Humidity Parameterization of the Navy Aerosol Model (NAM), Naval Research Laboratory, NRL report 8956, 1985.
- Ghude, S. D., Jena, C., Chate, D. M., Beig, G., Pfister, G. G., Kumar, R., and Ramanathan, V.: Reductions in India's crop yield due to ozone, *Geophys. Res. Lett.*, 41, 5685–5691, <https://doi.org/10.1002/2014GL060930>, 2014.
- Ghude, S. D., Chate, D. M., Jena, C., Beig, G., Kumar, R., Barth, M. C., Pfister, G. G., Fadnavis, S., and Pithani, P.: Premature mortality in India due to $PM_{2.5}$ and ozone exposure, *Geophys. Res. Lett.*, 43, 4650–4658, <https://doi.org/10.1002/2016GL068949>, 2016.
- Glotfelty, T., Zhang, Y., Karamchandani, P., and Streets, D. G.: Changes in future air quality, deposition, and aerosol-cloud interactions under future climate and emission scenarios, *Atmos. Environ.*, 139, 176–191, <https://doi.org/10.1016/j.atmosenv.2016.05.008>, 2016.
- Guenther, A., Monson, R., and Fall, R.: Isoprene and monoterpene rate variability: observations with Eucalyptus and emission rate algorithm development *J. Geophys. Res.*, 96, 10799–10808, 1991.
- Guenther, A., Karl, T., Harley, P., Wiedinmyer, C., Palmer, P. I., and Geron, C.: Estimates of global terrestrial isoprene emissions using MEGAN (Model of Emissions of Gases and Aerosols from Nature), *Atmos. Chem. Phys.*, 6, 3181–3210, <https://doi.org/10.5194/acp-6-3181-2006>, 2006.
- Hantson, S., Knorr, W., Schurgers, G., Pugh, T. A. M., and Arneth, A.: Global isoprene and monoterpene emissions under changing climate, vegetation, CO_2 and land use, *Atmos. Environ.*, 155, 35–45, <https://doi.org/10.1016/j.atmosenv.2017.02.010>, 2017.
- Heald, C. L., Henze, D. K., Horowitz, L. W., Feddema, J., Lamarque, J.-F., Guenther, A., Hess, P. G., Vitt, F., Seinfeld, J. H., Goldstein, A. H., and Fung, I.: Predicted change in global secondary organic aerosol concentrations in response to future climate, emissions, and land use change, *J. Geophys. Res.* 113, 2156–2202, <https://doi.org/10.1029/2007JD009092>, 2008.
- Hedegaard, G. B., Brandt, J., Christensen, J. H., Frohn, L. M., Geels, C., Hansen, K. M., and Stendel, M.: Impacts of climate change on air pollution levels in the Northern Hemisphere with special focus on Europe and the Arctic, *Atmos. Chem. Phys.*, 8, 3337–3367, <https://doi.org/10.5194/acp-8-3337-2008>, 2008.
- IEA: World Energy Outlook 2016 (WEO-2016), ISBN Print: 978-92-64-26494-6 / PDF: 978-92-64-26495-3, 2016.
- Jackson, M., Landgren, O., Benestad, R., Tayal, S., and Li, H.: The response of the hydrological system in India to climate change: focus on Lidder and Chandra catchments, in preparation, 2018.
- Jacob, D. and Winner, D.: Effect of climate change on air quality, *Atmos. Environ.*, 43, 51–63, <https://doi.org/10.1016/j.atmosenv.2008.09.051>, 2009.
- Jerrett, M., Burnett, R. T., Pope III, C. A., Ito, K., Thurston, G., Krewski, D., Shi, Y., Calle, E., and Thun, M.: Long-term ozone exposure and mortality, *N. Engl. J. Med.*, 360, 1085–1095, 2009.
- Jonson, J. E., Stohl, A., Fiore, A. M., Hess, P., Szopa, S., Wild, O., Zeng, G., Dentener, F. J., Lupu, A., Schultz, M. G., Duncan, B. N., Sudo, K., Wind, P., Schulz, M., Marmer, E., Cuvelier, C., Keating, T., Zuber, A., Valdebenito, A., Dorokhov, V., De Backer, H., Davies, J., Chen, G. H., Johnson, B., Tarasick, D. W., Stübi, R., Newchurch, M. J., von der Gathen, P., Steinbrecht, W., and Claude, H.: A multi-model analysis of vertical ozone profiles, *Atmos. Chem. Phys.*, 10, 5759–5783, <https://doi.org/10.5194/acp-10-5759-2010>, 2010.
- Jonson, J. E., Jalkanen, J. P., Johansson, L., Gauss, M., and Denier van der Gon, H. A. C.: Model calculations of the effects of present and future emissions of air pollutants from shipping in the Baltic Sea and the North Sea, *Atmos. Chem. Phys.*, 15, 783–798, <https://doi.org/10.5194/acp-15-783-2015>, 2015a.
- Jonson, J., Semeena, V., and Simpson, D.: Global ozone bias Trans-boundary particulate matter, photo-oxidants, acidifying and eutrophying components. Status Report 1/2015, The Norwegian Meteorological Institute, Oslo, Norway, 115–128, ISSN 1504-6109, 2015b.

- Kumar, R., Naja, M., Pfister, G. G., Barth, M. C., Wiedinmyer, C., and Brasseur, G. P.: Simulations over South Asia using the Weather Research and Forecasting model with Chemistry (WRF-Chem): chemistry evaluation and initial results, *Geosci. Model Dev.*, 5, 619–648, <https://doi.org/10.5194/gmd-5-619-2012>, 2012.
- Lacressonière, G., Foret, G., Beekmann, M., Siour, G., Engardt, M., Gauss, M., Watson, L., Andersson, C., Colette, A., Josse, B., Marécal, V., Nyiri, A., and Vautard, R.: Impacts of regional climate change on air quality projections and associated uncertainties, *Climatic Change*, 1, 1–16, <https://doi.org/10.1007/s10584-016-1619-z>, 2016.
- Langner, J., Bergström, R., and Foltescu, V.: Impact of climate change on surface ozone and deposition of sulphur and nitrogen in Europe, *Atmos. Environ.*, 39, 1129–1141, 2005.
- Langner, J., Engardt, M., Baklanov, A., Christensen, J. H., Gauss, M., Geels, C., Hedegaard, G. B., Nuterman, R., Simpson, D., Soares, J., Sofiev, M., Wind, P., and Zakey, A.: A multi-model study of impacts of climate change on surface ozone in Europe, *Atmos. Chem. Phys.*, 12, 10423–10440, <https://doi.org/10.5194/acp-12-10423-2012>, 2012.
- Lelieveld, J., Barlas, C., Giannadaki, D., and Pozzer, A.: Model calculated global, regional and megacity premature mortality due to air pollution, *Atmos. Chem. Phys.*, 13, 7023–7037, <https://doi.org/10.5194/acp-13-7023-2013>, 2013.
- Lelieveld, J., Evans, J. S., Fnais, M., Giannadaki, D., and Pozzer, A.: The contribution of outdoor air pollution sources to premature mortality on a global scale, *Nature*, 525, 367–371, <https://doi.org/10.1038/nature15371>, 2015.
- Lim, S. S., Vos, T., Flaxman, A. D., et al.: A comparative risk assessment of burden of disease and injury attributable to 67 risk factors and risk factor clusters in 21 regions, 1990–2010: a systematic analysis for the Global Burden of Disease Study 2010, *Lancet*, 380, 2224–2260, [https://doi.org/10.1016/S0140-6736\(12\)61766-8](https://doi.org/10.1016/S0140-6736(12)61766-8), 2012.
- Logan, J. A.: An analysis of ozonesonde data for the troposphere: Recommendations for testing 3-D models and development of a gridded climatology for tropospheric ozone, *J. Geophys. Res.*, 10, 16115–16149, 1998.
- Loibl, W., Winiwarter, W., Kopsca, A., Zufger, J., and Baumann, R.: Estimating the spatial distribution of ozone concentrations in complex terrain, *Atmos. Environ.*, 28, 2557–2566, 1994.
- Mahajan, A. S., De Smedt, I., Biswas, M. S., Ghude, S., Fadnavis, S., Roy, C., and van Roozendael, M.: Inter-annual variations in satellite observations of nitrogen dioxide and formaldehyde over India, *Atmos. Environ.*, 116, 194–201, <https://doi.org/10.1016/j.atmosenv.2015.06.004>, 2015.
- Mallik, C. and Lal, S.: Seasonal characteristics of SO₂, NO₂, and CO emissions in and around the Indo-Gangetic Plain, *Environ. Monit. Assess.*, 186, 1295–1310, <https://doi.org/10.1007/s10661-013-3458-y>, 2014.
- Mills, G., Hayes, F., Simpson, D., Emberson, L., Norris, D., Harmens, H., and Büker, P.: Evidence of widespread effects of ozone on crops and (semi-) natural vegetation in Europe (1990–2006) in relation to AOT40- and flux-based risk maps, *Global Change Biol.*, 17, 592–613, 2011.
- Ministry of Environment and Forests (Government of India): Climate Change and India: A 4X4 Assessment (A Sectorial and Regional Analysis for 2030s), 2010.
- Monks, P. S., Archibald, A. T., Colette, A., Cooper, O., Coyle, M., Derwent, R., Fowler, D., Granier, C., Law, K. S., Mills, G. E., Stevenson, D. S., Tarasova, O., Thouret, V., von Schneidemesser, E., Sommariva, R., Wild, O., and Williams, M. L.: Tropospheric ozone and its precursors from the urban to the global scale from air quality to short-lived climate forcer, *Atmos. Chem. Phys.*, 15, 8889–8973, <https://doi.org/10.5194/acp-15-8889-2015>, 2015.
- Morgan, P. B., Mies, T. A., Bollero, G. A., Nelson, R. L., and Long, S. P.: Season-long elevation of ozone concentration to projected 2050 levels under fully open-air conditions substantially decreases the growth and production of soybean, *New Phytol.*, 170, 333–343, 2006.
- Orru, H., Andersson, C., Ebi, K. L., Langner, J., Åström, C., and Forsberg, B.: Impact of climate change on ozone-related mortality and morbidity in Europe, *Eur. Respir. J.*, 41, 285–294, <https://doi.org/10.1183/09031936.00210411>, 2013.
- Pleim, J. and Ching, J.: Interpretive analysis of observed and modelled mesoscale ozone photochemistry in areas with numerous point sources, *Atmos. Environ.*, 27, 999–1017, 1993.
- Pommier, M., Clerbaux, C., and Coheur, P.-F.: Determination of enhancement ratios of HCOOH relative to CO in biomass burning plumes by the Infrared Atmospheric Sounding Interferometer (IASI), *Atmos. Chem. Phys.*, 17, 11089–11105, <https://doi.org/10.5194/acp-17-11089-2017>, 2017.
- Riahi, K., Rao, S., Krey, V., Cho, C., Chirkov, V., Fischer, G., Kindermann, G., Nakicenovic, N., and Rafaj, P.: RCP 8.5-A scenario of comparatively high greenhouse gas emissions, *Climatic Change*, 109, 33–57, <https://doi.org/10.1007/s10584-011-0149-y>, 2011.
- Saikawa, E., Trail, M., Zhong, M., Wu, Q., Young, C. L., Janssens-Maenhout, G., Klimont, Z., Wagner, F., Kurokawa, J., Nagpure, A. S., and Gurjar, B. R.: Uncertainties in emissions estimates of greenhouse gases and air pollutants in India and their impacts on regional air quality, *Environ. Res. Lett.*, 12, 065002, <https://doi.org/10.1088/1748-9326/aa6cb4>, 2017.
- Sharma S. and Kumar, A.: Air pollutant emissions scenario for India, The Energy and Resources Institute, New Delhi, India, ISBN 978-81-7993-639-9, 2016.
- Sharma S., Chatani S., Mahtta R., Goel A., and Kumar A.: Sensitivity analysis of ground level ozone in India using WRF-CMAQ models, *Atmos. Environ.*, 131, 29–40, 2016.
- Sharma, S. and Khare, M.: Simulating ozone concentrations using precursor emission inventories in Delhi – National Capital Region of India, *Atmos. Environ.*, 151, 117–132, 2017.
- Sharma, S., Sharma, P., and Khare, M.: Photo-chemical transport modelling of tropospheric ozone: A review, *Atmos. Environ.*, 159, 34–54, 2017.
- Sillman, S., Logan, J., and Wofsy, S.: A regional scale model for ozone in the United States with subgrid representation of urban and power plant plumes, *J. Geophys. Res.*, 95, 5731–5748, 1990.
- Silva, R. A., West, J. J., Zhang, Y., Anenberg, S. C., Lamarque, J.-F., Shindell, D. T., Collins, W. J., Dalsoren, S., Faluvegi, G., Folberth, G., Horowitz, L. W., Nagashima, T., Naik, V., Rumbold, S., Skeie, R., Sudo, K., Takemura, T., Bergmann, D., Cameron-Smith, P., Cionni, I., Doherty, R. M., Eyring, V., Josse, B., MacKenzie, I. A., Plummer, D., Righi, M., Stevenson, D. S., Strode, S., Szopa, S., and Zeng, G.: Global premature mortality due to anthropogenic outdoor air pollution and the contri-

- bution of past climate change, *Environ. Res. Lett.*, 8, 034005, <https://doi.org/10.1088/1748-9326/8/3/034005>, 2013.
- Simpson, D., Tuovinen, J.-P., Emberson, L., and Ashmore, M.: Characteristics of an ozone deposition module II: sensitivity analysis, *Water Air Soil Pollut.*, 143, 123–137, 2003.
- Simpson, D., Benedictow, A., Berge, H., Bergström, R., Emberson, L. D., Fagerli, H., Flechard, C. R., Hayman, G. D., Gauss, M., Jonson, J. E., Jenkin, M. E., Nyíri, A., Richter, C., Semeena, V. S., Tsyrö, S., Tuovinen, J.-P., Valdebenito, Á., and Wind, P.: The EMEP MSC-W chemical transport model – technical description, *Atmos. Chem. Phys.*, 12, 7825–7865, <https://doi.org/10.5194/acp-12-7825-2012>, 2012.
- Simpson, D., Andersson, C., Christensen, J. H., Engardt, M., Geels, C., Nyíri, A., Posch, M., Soares, J., Sofiev, M., Wind, P., and Langner, J.: Impacts of climate and emission changes on nitrogen deposition in Europe: a multi-model study, *Atmos. Chem. Phys.*, 14, 6995–7017, <https://doi.org/10.5194/acp-14-6995-2014>, 2014.
- Simpson, D., Tsyrö, S., and Wind, P.: Updates to the EMEP/MSC-W model, Transboundary particulate matter, photo-oxidants, acidifying and eutrophying components. EMEP Status Report 1/2015, The Norwegian Meteorological Institute, Oslo, Norway, 2015, 129–138, ISSN 1504-6109, 2015.
- Simpson, D., Nyíri, A., Tsyrö, S., Valdebenito, Á., and Wind, P.: Updates to the EMEP/MSC-W model, 2015–2016 Transboundary particulate matter, photo-oxidants, acidifying and eutrophying components. EMEP Status Report 1/2016, The Norwegian Meteorological Institute, Oslo, Norway, 2016, 133–139, ISSN 1504-6109, http://emeep.int/publ/reports/2016/EMEP_Status_Report_1_2016.pdf, 2016.
- Sinha, V., Kumar, V., and Sarkar, C.: Chemical composition of pre-monsoon air in the Indo-Gangetic Plain measured using a new air quality facility and PTR-MS: high surface ozone and strong influence of biomass burning, *Atmos. Chem. Phys.*, 14, 5921–5941, <https://doi.org/10.5194/acp-14-5921-2014>, 2014.
- Stadtler, S., Simpson, D., Schröder, S., Taraborrelli, D., Bott, A., and Schultz, M.: Ozone Impacts of Gas-Aerosol Uptake in Global Chemistry Transport Models, *Atmos. Chem. Phys. Discuss.*, <https://doi.org/10.5194/acp-2017-566>, in review, 2017.
- Surendran, D. E., Ghude, S. D., Beig, G., Emmons, L. K., Jena, C., Kumar, R., Pfister, G. G., and Chate, D. M.: Air quality simulation over South Asia using Hemispheric Transport of Air Pollution version-2 (HTAP-v2) emission inventory and Model for Ozone and Related chemical Tracers (MOZART-4), *Atmos. Environ.*, 122, 157–372, <https://doi.org/10.1016/j.atmosenv.2015.08.023>, 2015.
- Tiwari, S., Tunved, P., Hopke, P. K., Srivastava, A. K., Bisht, D. S., and Pandey, A. K.: Observations of ambient trace gas and PM10 concentrations at Patna, Central Ganga Basin during 2013–2014: The influence of meteorological variables on atmospheric pollutants, *Atmos. Res.*, 180, 138–149, <https://doi.org/10.1016/j.atmosres.2016.05.017>, 2016.
- Trail, M., Tsimpidi, A. P., Liu, P., Tsigaridis, K., Rudokas, J., Miller, P., Nenes, A., Hu, Y., and Russell, A. G.: Sensitivity of air quality to potential future climate change and emissions in the United States and major cities, *Atmos. Environ.*, 94, 552–563, 2014.
- Tsigaridis, K. and Kanakidou, M.: Secondary organic aerosol importance in the future atmosphere, *Atmos. Environ.*, 41, 4682–4692, <https://doi.org/10.1016/j.atmosenv.2007.03.045>, 2007.
- Tuovinen, J.-P., Ashmore, M., Emberson, L., and Simpson, D.: Testing and improving the EMEP ozone deposition module, *Atmos. Environ.*, 38, 2373–2385, 2004.
- Tuovinen, J.-P., Simpson, D., Ashmore, M., Emberson, L., and Gerosa, G.: Robustness of modelled ozone exposures and doses, *Environ. Pollut.*, 146, 578–586, 2007.
- Tuovinen, J.-P., Emberson, L., and Simpson, D.: Modelling ozone fluxes to forests for risk assessment: status and prospects, *Ann. For. Sci.*, 66, 401, <https://doi.org/10.1051/forest/2009024>, 2009.
- UNICEF: Clear the Air for Children – Report, ISBN: 978-92-806-4854-6, available at: <http://weshare.unicef.org/Package/2AMZIFKPWU1> (last access: 21 December 2017), 2016.
- van der Werf, G. R., Randerson, J. T., Giglio, L., Collatz, G. J., Mu, M., Kasibhatla, P. S., Morton, D. C., DeFries, R. S., Jin, Y., and van Leeuwen, T. T.: Global fire emissions and the contribution of deforestation, savanna, forest, agricultural, and peat fires (1997–2009), *Atmos. Chem. Phys.*, 10, 11707–11735, <https://doi.org/10.5194/acp-10-11707-2010>, 2010.
- van Loon, M., Vautard, R., Schaap, M., Bergstrom, R., Bessagnet, B., Brandt, J., Builjtjes, P. H. J., Christensen, J. H., Cuvelier, C., Graff, A., Jonson, J. E., Krol, M., Langner, J., Roberts, P., Rouil, L., Stern, R., Tarrason, L., Thunis, P., Vignati, E., White, L., and Wind, P.: Evaluation of long-term ozone simulations from seven regional air quality models, their ensemble, *Atmos. Environ.*, 41, 2083–2097, <https://doi.org/10.1016/j.atmosenv.2006.10.073>, 2007.
- WHO (World Health Organization): Methods and data sources for country-level causes of death 2000–2012, World Health Organ., Geneva, Switzerland, 2014.
- Wiedinmyer, C., Yokelson, R. J., and Gullette B. K.: Global Emissions of Trace Gases, Particulate Matter, and Hazardous Air Pollutants from Open Burning of Domestic Waste, *Environ. Sci. Technol.*, 48, 9523–9530, <https://doi.org/10.1021/es502250z>, 2014.
- Wild, O., Fiore, A. M., Shindell, D. T., Doherty, R. M., Collins, W. J., Dentener, F. J., Schultz, M. G., Gong, S., MacKenzie, I. A., Zeng, G., Hess, P., Duncan, B. N., Bergmann, D. J., Szopa, S., Jonson, J. E., Keating, T. J., and Zuber, A.: Modelling future changes in surface ozone: a parameterized approach, *Atmos. Chem. Phys.*, 12, 2037–2054, <https://doi.org/10.5194/acp-12-2037-2012>, 2012.
- Wu, S., Mickley, L. J., Kaplan, J. O., and Jacob, D. J.: Impacts of changes in land use and land cover on atmospheric chemistry and air quality over the 21st century, *Atmos. Chem. Phys.*, 12, 1597–1609, <https://doi.org/10.5194/acp-12-1597-2012>, 2012.
- Xin, Y. J., Wang, G. C., and Chen, L.: Identification of Long-Range Transport Pathways and Potential Sources of PM₁₀ in Tibetan Plateau Uplift Area: Case Study of Xining, China in 2014, *Aerosol Air Qual. Res.*, 16, 1044–1054, <https://doi.org/10.4209/aaqr.2015.05.0296>, 2016.
- Xu, J. Z., Zhang, Q., Wang, Z. B., Yu, G. M., Ge, X. L., and Qin, X.: Chemical composition and size distribution of summertime PM_{2.5} at a high altitude remote location in the northeast of the Qinghai–Xizang (Tibet) Plateau: insights into aerosol sources and processing in free troposphere, *Atmos. Chem. Phys.*, 15, 5069–5081, <https://doi.org/10.5194/acp-15-5069-2015>, 2015.
- Young, P. J., Arneth, A., Schurges, G., Zeng, G., and Pyle, J. A.: The CO₂ inhibition of terrestrial isoprene emission significantly

- affects future ozone projections, *Atmos. Chem. Phys.*, 9, 2793–2803, <https://doi.org/10.5194/acp-9-2793-2009>, 2009.
- Zhang, Y., Bowden, J. H., Adelman, Z., Naik, V., Horowitz, L. W., Smith, S. J., and West, J. J.: Co-benefits of global and regional greenhouse gas mitigation for US air quality in 2050, *Atmos. Chem. Phys.*, 16, 9533–9548, <https://doi.org/10.5194/acp-16-9533-2016>, 2016.